

# ESA GaN Noise Assessment - Summary Report

QINETIQ/S&E/OPC/CR041056/1.0

Copy of 60

Cover + xi + 42 pages

April 2004

A R Barnes

## Unlimited

### Customer Information

Customer Reference Number	A0/1-3916/01/NL/CK
Project Title	ESA GaN Noise Assessment
Company Name	ESA
Customer Contact	F Garat
Contract Number	ESTEC Contract No. 15908/01/NL/CK
Milestone Number	8
Date Due (dd/mm/yyyy)	30/04/2004

This Document was produced by QinetiQ for ESA Under Order/Contract reference  
15908/01/NL/CK

© Copyright of QinetiQ ltd 2004

Approval for wider use of releases must be sought from:

Intellectual Property Department, QinetiQ ltd, Cody Technology Park, Farnborough,  
Hampshire GU14 0LX

**Authorisation**

**Prepared by** A R Barnes  
**Title** Technical Leader MMIC & RF Sub-systems  
**Signature**  
**Date** April 2004  
**Location** PA113

**Authorised by** M Astles  
**Title** Project Manager  
**Signature**  
**Date**

Record of changes

Issue	Date	Detail of Changes
1.0	April 2004	First issue

**Abstract**

This report summarises the key results from the ESA project “Noise Assessment of Gallium Nitride Structures” (reference A0/1-3916/01/NL/CK) covering the period from May 2002 to January 2004. The objective of this work programme was to perform a study of GaN field effect transistors in order to gain an improved understanding of the intrinsic noise sources. Three different material growth variants have been characterised during the course of this work to determine their RF and low frequency noise properties. Additional work items have included a system study to evaluate the benefits of using GaN for realising an L-band Tx/Rx module and evaluation of the phase noise performance of a 10GHz oscillator.

## Executive summary

Wide bandgap semiconductors have many properties (e.g. a bandgap that allows optical transmission and an exceptionally high breakdown field) that are near ideal for electronic and optical applications requiring high temperature, high frequency, high power and radiation hardness. To date most researchers have concentrated their efforts on examining the high frequency output power capability of transistors and in developing light emitting diodes (LED's) manufactured using the gallium nitride (GaN) material base. To the surprise of many workers in the field, recent measurement results have also shown that GaN offers great potential for low noise applications. The multiple attributes of GaN transistors (i.e. simultaneous low noise and high power performance) has stimulated considerable system interest for realising high performance transmit receive (Tx/Rx) module front-ends.

This report summarises the key results from the ESA project "Noise Assessment of Gallium Nitride Structures" (reference A0/1-3916/01/NL/CK) covering the period from May 2002 to January 2004. The objective of this work programme was to perform a study of GaN field effect transistors in order to gain an improved understanding of the intrinsic noise sources and to assess the capability of GaN for use in high performance receivers.

Three different material growth systems have been characterised during the course of this work to determine their RF and low frequency noise properties. These were MOVPE growth on SiC, including two layer variants (variant 1 (GaN/AlGaIn) and variant 2 (GaN/AlN/AlGaIn)), MOVPE growth on sapphire and MBE growth on sapphire. Additional work items have included a system study to evaluate the benefits of using GaN for realising an L-band Tx/Rx module and evaluation of the phase noise performance of a 10GHz oscillator.

- This work has shown that GaN device technology offers gain and noise performance comparable to that achievable with GaAs, but with breakdown voltages exceeding 60V. These results suggest an important new application area for GaN as robust low-noise amplifiers, where the high breakdown voltage offers the potential for removal of front-end protection devices.
- System simulation has shown that it could be feasible to remove the limiter and possibly the circulator functions for an L-band phased array radar system with advantages in terms of system noise figure, component cost and mass.
- However, experimental overdrive measurements have shown that there may be a soft breakdown effect that needs to be resolved before the full potential of GaN based receivers can be realised.
- Low frequency noise and oscillator phase noise measurements have given an indication of the status of processing/material quality compared with mature device technologies such as GaAs and SiGe. It is clear that improvements in material growth and device process technology are still required.
- **Over time however, these material improvements are likely to occur and it is therefore concluded that GaN offers exciting possibilities for realising high power amplifiers and highly robust receiver front-ends.**

**List of contents**

<b>Authorisation</b>	<b>iii</b>
<b>Record of changes</b>	<b>iv</b>
<b>Abstract</b>	<b>v</b>
<b>Executive summary</b>	<b>vi</b>
<b>List of contents</b>	<b>vii</b>
<b>List of Tables</b>	<b>ix</b>
<b>List of Figures</b>	<b>x</b>
<b>1 Introduction</b>	<b>1</b>
<b>2 Device variants examined (WP 1400)</b>	<b>2</b>
2.1 Material growth options	2
2.2 Substrate options	2
2.3 Growth and material variants used for evaluation	2
2.4 MOVPE grown AlGa <sub>N</sub>	3
2.5 MBE grown AlGa <sub>N</sub> /Ga <sub>N</sub>	3
<b>3 RF characterisation (WP 2100)</b>	<b>4</b>
3.1 S-parameter and noise parameter measurements	4
<b>4 High frequency noise assessment (WP 2200)</b>	<b>6</b>
4.1 Background	6
4.2 Modelling	6
4.3 Physical interpretation for the RF noise sources	8
<b>5 Overdrive test results (WP 2300 – Part 1)</b>	<b>10</b>
5.1 Rationale	10
5.2 Test procedure	10
5.3 DC gate-source and gate-drain breakdown measurements	11
5.4 Continuation of RF overdrive measurements	12
5.5 Summary of key results from overdrive testing	12
<b>6 Transmit receive module system simulation (WP 2300 – Part 2)</b>	<b>13</b>

6.1	TRM modelling	13
6.2	Amplifier model	13
6.3	TRM description	13
6.4	TRM ADS model	13
<b>7</b>	<b>Low frequency noise (WP 3100 and WP 3200)</b>	<b>15</b>
7.1	Rationale	15
7.2	Measurement of low frequency drain and gate current noise	15
7.3	Low frequency noise modelling	16
<b>8</b>	<b>Oscillator phase noise comparison (WP 3300)</b>	<b>17</b>
8.1	Rationale	17
8.2	Choice of active device	17
8.3	Oscillator topology	18
8.4	Measured results	18
<b>9</b>	<b>Conclusions</b>	<b>20</b>
<b>10</b>	<b>Acknowledgements</b>	<b>24</b>
<b>11</b>	<b>References</b>	<b>25</b>
<b>12</b>	<b>Tables</b>	<b>26</b>
<b>13</b>	<b>Figures</b>	<b>29</b>
	<b>Report documentation page</b>	<b>41</b>

**List of Tables**

Table 12-1; Device structures examined	26
Table 12-2; Summary of MOVPE device performance (Variant 1)	26
Table 12-3; Summary of MBE device performance	26
Table 12-4; Gate and drain noise current source strength versus $I_{ds}$ (MOVPE on SiC variant 1)	27
Table 12-5; Gate and drain noise current source strength versus $I_{ds}$ (MOVPE on SiC variant 2)	27
Table 12-6; Gate and drain noise current source strength versus $I_{ds}$ (MBE on sapphire)	28
Table 12-7; Publication analysis for low noise GaN devices (for sub-references see [4])	28
Table 12-8; Summary of oscillator measurement results	28

List of Figures

Figure 13-1; Photograph of Bookham device field (MOVPE on SiC)	29
Figure 13-2; Photograph of Madrid University device field (MBE on sapphire)	29
Figure 13-3; S-parameter data for MOVPE device on SiC (variant 1, Vds=20V, Vgs=-10V, T=25°C)	30
Figure 13-4; S-parameter data for MOVPE device on sapphire (variant 1, Vds=10V, Vgs=-4V, T=25°C)	31
Figure 13-5; S-parameter data for MBE device on sapphire (4Un75, Vds=15V, Vgs=-7V, T=25°C)	32
Figure 13-6; NFmin and associated gain for MOVPE device on SiC, Variant 1 (Vds=20V, T=25°C)	33
Figure 13-7; Schematic of HFET model used for noise and S-parameter analysis	34
Figure 13-8; Typical transmit-receive architecture	34
Figure 13-9; Gate-source breakdown behaviour for MOVPE device on SiC, Variant 1 (22.36 3G1)	35
Figure 13-10; Gate-drain breakdown behaviour for MOVPE device on SiC, Variant 1 (22.36 3G1)	35
Figure 13-11; Gate-drain breakdown voltage behaviour for Bookham H40P GaAs pHEMT	35
Figure 13-12; Example photograph showing typical gate finger failure during isolation testing	36
Figure 13-13; Simulated GaN LNA noise figure/gain (stabilised, transformer matching network)	36
Figure 13-14; Astrium L-band SAR radar diagram (including circulator and limiter)	37
Figure 13-15; Experimental set-up for LF drain current noise measurements	37
Figure 13-16; Typical drain current noise spectral density with Ids at Vgs=0 (MOVPE device on sapphire)	38
Figure 13-17; Comparison of Hooge parameter ( $\alpha_H$ ) for each device technology	38
Figure 13-18; Typical variation in gate current noise spectral density with Vgs, Vds=0V (MOVPE device on sapphire, Ig varying from -1.2nA to -0.24µA)	39
Figure 13-19; Aluminium nitride drop-in carrier containing GaN device	39
Figure 13-20; Photograph of 10GHz oscillator breadboard	40
Figure 13-21; Oscillator phase noise using SiGe bipolar, GaAs pHEMT and 2 GaN HFET on SiC variants	40

## 1 Introduction

- 1.1 Wide bandgap semiconductors have many properties (e.g. a bandgap that allows optical transmission and an exceptionally high breakdown field) that are near ideal for electronic and optical applications requiring high temperature, high frequency, high power and radiation hardness. To date most researchers have concentrated their efforts on examining the high frequency output power capability of transistors and light emitting diodes (LED's) manufactured using the gallium nitride (GaN) material base. To the surprise of many workers in the field, recent measurement results have also shown that GaN offers great potential for low noise applications. The multiple attributes of GaN transistors (i.e. simultaneous low noise and high power performance) has stimulated considerable system interest for realising high performance transmit receive (Tx/Rx) module front-ends.
- 1.2 In April 2002 QinetiQ was successful in tendering for a European Space Agency (ESA) contract to investigate the advantages offered by GaN for realising space based Tx/Rx modules. This ESA project was entitled "Noise Assessment of Gallium Nitride Structures" (reference A0/1-3916/01/NL/CK). The objective of this work programme was to perform a study of GaN field effect transistors in order to gain an improved understanding of the intrinsic noise sources. In particular the noise properties of three different material growth variants have been examined during the course of this work, MOVPE growth on SiC, MOVPE growth on sapphire and MBE growth on sapphire. Additional work items have included a system study to evaluate the benefits of using GaN for realising an L-band Tx/Rx module and evaluation of the phase noise performance of a 10GHz oscillator.
- 1.3 There are a number of sub-contractors that QinetiQ has worked with to ensure successful completion of this project, namely:
- IXL : Responsible for low frequency noise assessment/modelling
  - phconsult : Responsible for high frequency noise modelling
  - Astrium : Responsible for performing the system simulation study
- 1.4 Collaboration was established with the University of Madrid, who supplied the electron-beam defined transistors fabricated on MBE grown GaN on sapphire.
- 1.5 This report summarises the key project findings over the period May 2002 to January 2004. The report is divided into 9 main sections. Section 1 gives a short introduction describing the aims of the project. In section 2, the material growth and device variants used for evaluation are described, while in section 3 RF characterisation results are presented. Section 4 discusses the results from high frequency noise modelling and their interpretation. In section 5, the suitability of GaN for use in a system environment with and without protection devices has been analysed. In particular, experimental RF overdrive results and a CAD system simulation of an L-band radar system are presented in this section. Low frequency noise measurements and their interpretation are given in section 7, while in section 8 phase noise results for a GaN based oscillator are described.

Finally, in section 9, conclusions on the suitability of GaN for realising high performance receiver front-ends are presented along with recommendations for future work.

## **2 Device variants examined (WP 1400)**

### **2.1 Material growth options**

2.1.1 A variety of different growth techniques can be employed to grow GaN epitaxially. Three main variants are currently used;

- Metal Organic Vapour Phase Epitaxy (MOVPE)
- Molecular Beam Epitaxy (MBE)
- Hydride Vapour Phase Epitaxy (HVPE)

2.1.2 MOVPE uses chemical precursor gases that are decomposed and reacted on the surface of a heated substrate. By comparison, MBE uses a high vacuum system to co-evaporate the layer materials. Growth is generally at a temperature lower than that used in MOVPE, but with equally complex growth processes. Because of problems with initiating growth, MBE is frequently carried out on an MOVPE grown template layer.

2.1.3 HVPE is another chemical vapour deposition system, but is capable of high growth rates. Indeed, this has been used to grow sufficiently thick layers that they can be used as growth substrates. In general though, this latter technique has not yet been used successfully to form high quality layers and hence MBE and MOVPE are the preferred growth techniques.

2.1.4 To-date there is no clear optimum choice between MBE and MOVPE with excellent device results reported for both techniques.

### **2.2 Substrate options**

2.2.1 Another significant factor affecting device performance is the choice of the substrate growth material. Single crystal GaN is not available in sizes larger than a few millimetres. As a result, hetero-epitaxial growth of GaN has had to be developed on non-lattice matched materials, in particular sapphire, silicon carbide (SiC) and silicon. Sapphire has primarily been used at the research stage of GaN development, SiC for best thermal conductivity and silicon for (future) low cost production.

### **2.3 Growth and material variants used for evaluation**

2.3.1 A key objective of this ESA work programme has been to compare and contrast the performance of GaN devices grown using different epitaxy techniques and fabricated on different substrate materials. Three growth/material systems were originally proposed for evaluation:

- 1) MOVPE epitaxy with devices fabricated on silicon carbide (SiC)

- 2) MOVPE epitaxy with devices fabricated on sapphire
- 3) MBE epitaxy with devices fabricated on sapphire

2.3.2 The original intention was to process HFET devices on SiC at QinetiQ using a newly developed 0.25 $\mu\text{m}$  gate length e-beam lithography fabrication process. Unfortunately, there were delays in establishing this process. Therefore a decision was made to perform initial comparison measurements on 0.25 $\mu\text{m}$  gate length transistors fabricated by Bookham Technology, but using QinetiQ supplied MOVPE starting material (variant 1). Later on in the project, QinetiQ device samples incorporating an aluminium nitride exclusion layer (variant 2) became available and were also characterised. Table 12-1 summarises all the device types examined during the course of this work. A description of the active device details is also given in 2.4 and 2.5 for each device type respectively.

## 2.4 MOVPE grown AlGaN

**Variant 1:** The first device variant used 30nm, 25% undoped AlGaN on a 1.2 $\mu\text{m}$  undoped insulating GaN layer. The 2x50 $\mu\text{m}$  0.2 $\mu\text{m}$  Pt/Au T-gate devices were fabricated at Bookham Technology in 2001. The source-drain gap was 3 $\mu\text{m}$ . A photograph of the field pattern for this device variant is given in figure 13-1. This device structure was evaluated with both silicon carbide (SiC) and sapphire substrates. On SiC there were  $1.0 \times 10^{13} \text{cm}^{-2}$  carriers and a sheet resistance of 520 $\Omega$ /square, whereas on sapphire there were  $8.1 \times 10^{12} \text{cm}^{-2}$  carriers and a sheet resistance of 619 $\Omega$ /square.

2.4.1 **Variant 2:** The second technology had a similar layer structure, except that it included a  $\sim 1\text{nm}$  AlN layer at the GaN/AlGaN interface. The sheet charge was  $1.1 \times 10^{13} \text{cm}^{-2}$  and the sheet resistance was 300 $\Omega$ /square. The AlN layer included in variant 2 has the effect of increasing the barrier height between the GaN and AlGaN by more than 0.5eV and gives improved mobility. The devices using this second layer structure were fabricated at QinetiQ on SiC and had a 2x50 $\mu\text{m}$  0.3 $\mu\text{m}$  Ni/Au T-gate with a 3.5 $\mu\text{m}$  source-drain gap.

## 2.5 MBE grown AlGaIn/GaN

Two part wafers of MBE grown device samples on sapphire, with a 30nm  $\text{Al}_{0.25}\text{Ga}_{0.75}\text{In}$  Schottky layer, were obtained from Madrid University in April 2003. These samples had an electron beam written 0.6 $\mu\text{m}$  gate, a source-drain separation of 5 $\mu\text{m}$  and a gate width of 150 $\mu\text{m}$  (2x75 $\mu\text{m}$ ). A photograph of the field pattern for the MBE device variants is given in figure 13-2.

### 3 RF characterisation (WP 2100)

#### 3.1 S-parameter and noise parameter measurements

3.1.1 Multi-bias S-parameter measurements were made on each material variant over the dc to 50GHz frequency range and over the 25°C to 150°C temperature range. DC IV characteristics, Maximum Available Gain (MAG), unity gain cut-off frequency ( $f_t$ ) and maximum oscillation frequency ( $f_{max}$ ) information was derived from this data. A typical measurement set for an MOVPE grown device on sapphire and silicon carbide is given in figure 13-3 and 13-4 respectively. A reduction in drain-source current ( $I_{ds}$ ) with increasing drain source voltage ( $V_{ds}$ ) was observed for the devices fabricated on sapphire due to its poor thermal conductivity compared with SiC. Similar values were observed for  $f_t$  and  $f_{max}$  from all MOVPE grown device variants with values of  $\approx 32\text{GHz}$  and  $\approx 80\text{GHz}$  obtained respectively.

3.1.2 For the MBE grown device on sapphire, measurement characterisation concentrated on a  $2 \times 75\mu\text{m}$  gate width device since this was similar in size to devices characterised using MOVPE growth. Typical, small signal, measurement data for the MBE grown device is shown in figure 13-5. Lower values for  $f_t$  and  $f_{max}$  were obtained for this device variant, due to the longer gate length ( $0.6\mu\text{m}$ ), with values of  $\approx 18\text{GHz}$  and  $\approx 45\text{GHz}$  measured respectively.

3.1.3 RF on wafer (RFOW) noise parameter measurements were also undertaken to derive minimum noise figure and associated gain for each device variant as a function of frequency and bias. The noise figure measurements were performed over the 2 to 23GHz frequency range. Typical measured data for a  $2 \times 50\mu\text{m}$  MOVPE device grown on SiC is shown in figure 13-6. It can be seen that at 10GHz a minimum noise figure of  $\approx 1\text{dB}$  and an associated gain of  $>12\text{dB}$  was obtained.

- This is an excellent result for a device that is not optimised for low noise figure and is comparable to the noise performance achieved from equivalent GaAs MESFETs.

3.1.4 The noise figure performance for the MOVPE devices grown on sapphire was found to be inferior compared with the devices manufactured on SiC. However, it should be noted that only a limited set of samples, taken from the edge of the wafer, were available for noise assessment of the sapphire based devices. Therefore this result might not be statistically significant.

3.1.5 For the MBE grown device, a minimum noise figure of 4dB and an associated gain of 8dB was obtained at 10GHz ( $V_{ds}=15\text{V}$ ).

#### 3.1.6 Measurements over temperature

3.1.7 Transistor measurements were also made at elevated temperatures in order to determine if device performance changes significantly. RFOW S-parameter measurements were made using a thermal chuck and data recorded at discrete temperatures, 25°C, 50°C, 100°C, and 150°C. For the MOVPE devices fabricated on SiC, there was a small

variation in device S-parameters, primarily  $S_{21}$ , which was found to reduce by approximately 0.8dB at 150°C compared with operation at ambient temperature. It is worth noting that the changes observed in gain as a function of temperature are lower than would typically be observed with GaAs devices. A typical change in gain with temperature is quoted as being -0.015dB/°C for a GaAs transistor. For a temperature differential of 125 °C this corresponds to a gain change of approximately 1.9dB (1.1dB higher than observed with the GaN MOVPE device on SiC).

3.1.8 Performance measurements as a function of temperature were also made for the MOVPE devices grown on sapphire. In contrast to devices grown on SiC, it was found that operating temperature had a significant influence on device performance. Again this is felt to be due to the low thermal conductivity of sapphire. It was found that  $f_t$  and  $f_{max}$  were reduced to 13GHz and 37.7GHz respectively when operated at a temperature of 150°C. Similarly, MAG performance was degraded considerably, with a value of 8.5dB (down from 12.1dB) obtained at 150°C for an operating frequency of 10GHz.

- It is clear that the thermal performance of GaN devices grown on sapphire substrates is far inferior to those grown on SiC.

3.1.9 A summary comparison of measured RF performance is given in table 12-2 and 12-3 respectively for the MOVPE and MBE device growth variants.

## 4 High frequency noise assessment (WP 2200)

### 4.1 Background

4.1.1 A key objective of this work package has been to relate the measured noise parameters of GaN HFET devices to the underlying physical mechanisms of noise and hence to identify ways in which the device material structure and geometry could be changed in order to further improve noise performance. This has been achieved in two parts:

- a. Measured RF data has been used to derive a bias dependent noise model such that the fundamental high frequency noise mechanisms can be identified.
- b. This has then been followed by a literature review on published GaN device results, a consideration of the theoretical contributions of the noise sources and interpretation of the measured data.

### 4.2 Modelling

4.2.1 An equivalent circuit model, incorporating gate and drain current noise sources, was used to fit the measured S-parameter and noise data as shown in figure 13-7. At each bias point, the measured minimum noise figure as a function of frequency was used to determine the magnitudes of the noise sources. The dominant contributions to noise are felt to be due to the gate and drain current fluctuations, with any input voltage noise assumed to be due to thermal noise from the input resistors in the device model.

4.2.2 Equivalent circuit values used to fit the measured S-parameter data were derived in a consistent manner using a physics based fitting routine (FETLINK). These parameters then define the small signal equivalent circuit model, which in turn was used to derive the noise source magnitudes from the measured RF noise figure data.

#### 4.2.3 MOVPE growth on SiC (variant 1)

4.2.4 Above 12GHz it was found that the drain noise current was the major contribution to noise figure (i.e. for devices without a large gate leakage current). Below 10GHz, the relative importance of gate current and voltage noise sources can be deduced from the frequency dependence of the minimum noise figure ( $NF_{min}$ ). In most of the samples examined the current source contributions were the most important, with their magnitude deduced from  $NF_{min}$ .

4.2.5 Typical magnitudes for the gate current and drain current noise sources used to fit experimental data as a function of drain bias are given in table 12-4 for device variant 1. It can be seen that the drain current noise contribution  $\langle id^2 \rangle$  is typically 2 or 3 orders of magnitude higher than the gate noise  $\langle ig^2 \rangle$ . It was also found that the magnitude of the drain noise current source was very similar to that obtained from an equivalent GaAs pHEMT, particularly for low values of drain current. In addition it was observed that the drain noise contribution was essentially constant with increasing  $V_{ds}$ , whereas the gate

noise contribution was found to increase with  $V_{ds}$ . At low frequencies this would manifest itself as an increase in  $NF_{min}$  as  $V_{ds}$  is increased.

4.2.6 The main features of the noise sources required to fit the noise data for device variant 1 were as follows:

- The drain current source is independent of frequency and of drain voltage in the range 10-20V, and increases approximately linearly with drain current, but less rapidly than in a GaAs device of similar gate length. The magnitude of the noise for samples on SiC and for the best samples on sapphire is approximately 10% of that expected for ideal shot noise.
- The gate current noise sources are smaller than the drain noise source. They correspond approximately to shot noise produced by gate leakage currents of a few  $\mu A$ . In contrast to the magnitude of the gate noise source, which increases with  $V_{DS}$ , the measured DC gate leakage current increases with decreasing drain current (increasing magnitude of  $V_{GS}$ ), and is almost independent of  $V_{DS}$ . However, a more complicated noise source model is needed to simulate the observed increase in  $NF_{min}$  at frequencies below 5GHz.
- In general the model can describe the experimental results without any additional voltage noise sources, and without any correlation between the drain and gate noise sources.

#### 4.2.7 MBE growth on sapphire

4.2.8 The values of the drain current noise source were found to be comparable to those presented for device variant 1 (MOVPE growth on SiC). However, the most obvious feature of the data for this device sample was the much higher noise contribution from the gate current. Over an order of magnitude greater than in the variant 1 samples. This was not unexpected, since the gate leakage current was also found to be high in these devices ( $>70\mu A$ ).

#### 4.2.9 MOVPE growth on SiC (variant 2)

4.2.10 Measured values of the minimum noise figure were very low. For the largest negative gate bias voltages  $NF_{min}$  was negative, indicating problems with the measurement calibration. In spite of this problem, noise modelling could be carried out with reasonable accuracy for all bias values except  $V_{gs}=-7V$ . No significant gate current contributions were required in the fit, and there was a general increase of the magnitude of the drain current fluctuations with drain current at low currents, but the values saturate at higher drain currents. The dominant variation in the fitting parameters was the reduction of transconductance ( $g_m$ ) in this regime, much more marked than for the MBE or variant 1 samples. The analysis of a second QinetiQ sample (see below) suggests that there was a potential problem with the measurement of the S-parameters at  $V_{ds}=10V$  and with large drain currents in this sample. Therefore noise measurements on a second device (10-07) were also carried out.

4.2.11 Measurements on the second device sample (for  $V_{ds}=15V$  and  $V_{gs}=-2, -3$  and  $-4V$ ) could be analysed. Sensible results for both the equivalent circuit model parameters and the

noise sources were obtained which were more in line with those expected on the basis of earlier measurement data for a device of very similar geometry.

4.2.12 Tables 12-4, 12-5 and 12-6 respectively show the gate and drain noise current coefficients used to provide a fit to measured noise parameter data for the MOVPE (variant 1 and variant 2) and MBE device samples.

#### 4.2.13 Literature search

4.2.14 A number of publications on low noise GaN devices were examined during the course of this work in order to try and identify, compare and assess the intrinsic device noise sources [4].

4.2.15 The first important results were published by HRL, who are clearly developing devices in order to provide more robust LNAs. A number of their publications are analysed in table 12-7, together with other data. The table is incomplete because detailed device models were not available in all cases, but it is noticeable that the measured minimum noise figures are very similar in all cases ( $\approx 0.8\text{dB}$  to  $1.2\text{dB}$  at  $12\text{GHz}$ ). Of particular interest are the last four columns, where the data can be analysed to derive values for the magnitude of the drain noise current sources. The last two columns refer to two different device structures fabricated by HRL, with  $15\text{nm}$  and  $30\text{nm}$  Schottky AlGaIn barriers. The different values for  $NF_{\min}$  arise from the different values of  $g_m$ . It is interesting to note that the magnitude of the drain noise current sources derived from measurements on device variant 1 and 2, is similar to the values derived from published results (i.e. for low noise bias operation ( $V_{gs} = -6\text{V}$  to  $-7\text{V}$ )).

### 4.3 Physical interpretation for the RF noise sources

4.3.1 It is not straightforward to compare the results obtained from this project to allow a meaningful interpretation of the origin of the physical RF noise sources. Measurements on devices with longer gate lengths and with different concentrations of aluminium in the Schottky layer are required. Even so a number of important points can be noted:

- The main source of noise in a device without significant gate current leakage is the drain current. Although the magnitude of the drain current fluctuations is comparable to those in GaAs HEMTs, the lower gain of typical GaN devices means that at  $20\text{GHz}$  the input contact and series resistances contribute only about 10% of the total noise. A major improvement in noise performance will not result from lower input resistances, except for much shorter gate length devices with higher gain. The drain current noise is independent of temperature.
- A good Schottky contact is important to reduce the gate current. Shot noise arising from current through the Schottky barrier has a strong influence on the noise performance, particularly below  $10\text{GHz}$ . In general, the gate current should be below  $1\ \mu\text{A}$  in a low-noise device. A good Schottky contact is also important in terms of the robustness of the device. It is shown in section 5 that gate leakage current is the dominant cause of device failure under reverse bias conditions.
- There is an additional noise source, probably related to gate noise, which gives an increase in  $NF_{\min}$  at the lowest frequencies. The origin of this contribution has not

## Unlimited

been identified, but is clearly sample related, and so a consequence of the processing and not an intrinsic property of GaN HFETs.

- Measurements on additional devices and further analysis of the published literature are needed to identify the mechanisms behind the current noise fluctuations. The range of possible mechanisms for drain current fluctuations is too large to allow an unambiguous identification without further studies. Such an understanding is necessary to identify the preferred device structure and geometry, and the optimum bias points, for minimum noise operation. Depending on the application, a balance may be needed between the requirements for low noise and high power.

## 5 Overdrive test results (WP 2300 – Part 1)

### 5.1 Rationale

5.1.1 In section 3 it was shown that the high frequency noise performance of GaN based devices is comparable to that achievable from GaAs. These results suggest an important new application area for GaN as robust low-noise amplifiers, where the high breakdown voltage offers the potential for removal of front-end protection devices.

5.1.2 A typical schematic diagram for a radar transmit/receive front-end is shown in figure 13-8. This type of system usually includes a circulator, to provide some degree of transmit-receive isolation and a PIN diode limiter preceding a GaAs low noise amplifier (LNA). The limiter is used to prevent the sensitive receiver chain from being damaged by RF overload. If a GaN based LNA can be used instead of GaAs, it may be possible to remove the limiter and circulator functions with immediate system benefits:

- Removal of the limiter and circulator will allow a significant reduction in volume and mass. This is critical for space based applications.
- A reduction in cost can be achieved, particularly where multiple receive channels are needed (e.g. for space based synthetic aperture radar (SAR) systems), since there is a reduction in component count.
- The ohmic insertion loss of the limiter and circulator functions can be removed giving an improvement in system noise figure of 1 to 1.5dB (at L-band).

5.1.3 A key aim of this work package was to subject a GaN based LNA to RF overdrive conditions in order to ascertain the effects on device performance and to determine the feasibility of removing the limiter/circulator functions.

### 5.2 Test procedure

5.2.1 Due to the large quantity of available devices, it was agreed that all overdrive tests would be carried out on device variant 1 (MOVPE growth on SiC). A co-axial test jig was designed to accept drop-in carriers containing these device samples. The test jig was then used in conjunction with input and output tuners such that appropriate matching conditions were used to configure the device under test to operate as a 4GHz low noise amplifier. Under these conditions a small signal gain of 12dB and a noise figure of 3dB was typically achieved (NB: noise figure could be reduced further, however this was constrained due to the available tuning range).

5.2.2 A number of experiments were undertaken in which the level of stress applied to the device was gradually increased, ultimately leading to device destruction. Initially power transfer measurements were made with the device in its “on-state”, i.e. in its normal LNA mode of operation ( $V_{ds}=20V$ ,  $V_{gs}=-5V$ ). Typically a  $P_{1dB}$  compressed output power of 17dBm was obtained for this device size ( $2 \times 50 \mu m$ ). Next the device was turned off, i.e. emulating the LNA bias conditions during transmit, and subjected to increasing levels of

RF input power whilst monitoring its off state isolation. Initial investigations concentrated on examining the off-state power handling capability with the amplifier heavily biased beyond pinch-off ( $V_{gs} < -20V$ ) and with  $V_{ds} = 0V$  as this was expected to give the best performance.

5.2.3 After each successive overdrive measurement, the LNA was switched back to its “on-state” and re-measured to determine if there was any degradation in gain and output power. Unfortunately it was found that with increased RF overdrive stressing the devices suffered significant gain and output power degradation. Therefore it was decided to stop the overdrive measurements and undertake forward and reverse bias dc gate diode measurements to determine the device breakdown behaviour with increasing voltage stress.

### 5.3 DC gate-source and gate-drain breakdown measurements

5.3.1 Reverse bias measurements were made to determine both the gate-source and gate-drain diode characteristics. The devices initially behaved as expected with stable reverse-bias leakage current levels ( $\sim 1\mu A - 5\mu A$ ) up until a particular reverse-bias voltage threshold. Once the critical reverse-bias threshold voltage was reached the devices became more leaky and displayed a leakage current plateau for applied voltages of  $< -8V$  (i.e. a similar magnitude to the pinch-off voltage).

5.3.2 A typical forward and reverse bias (gate-source) diode plot is shown in figure 13-9, where the trace numbers (in brackets) show the measurement order. The first trace,  $I_g(1)$ , was measured up to  $V_{gs} = -25V$  and the gate-source diode  $I_g - V_{gs}$  curve is repeatable and stable. For higher reverse bias, at around  $V_{gs} = -29V$ , a critical voltage is reached and there is a sharp increase in gate current up to the  $100\mu A$  compliance limit. Later traces (2, 3, 4 and 5) then show increasing leakage current as the device is further stressed. Note that the forward diode measurements were taken first and show gate current values up to  $I_g = \sim 10mA$ , an order of magnitude higher than in reverse bias. Forward gate current did not appear to degrade the device in terms of the reverse leakage current.

5.3.3 Similar behaviour was observed for the gate-drain diode as shown in figure 13-10.

5.3.4 For comparison, DC breakdown measurements were also performed on a Bookham H40P GaAs PHEMT device of similar geometry and size. The H40P device has a  $0.25\mu m$  gate length, a source-drain spacing of  $3\mu m$  and a source-gate spacing of  $\sim 1\mu m$ . The dc gate-drain breakdown results are shown in figure 13-11 and show the opposite effect compared to the GaN devices. That is, the gate leakage currents reduce with increasing bias stress (similar to a burn-in period) and then stabilise. However, note that the onset of breakdown for the H40P GaAs device gate-source diode occurs at  $V_{gs} = -12V$ , which is approximately half that of the GaN device examined ( $V_{gs} = -25V$  to  $-30V$ ). Furthermore, the transistor I-V curve was found to remain unchanged after successive reverse bias measurements. This was not the case for the GaN devices once the critical threshold voltage had been passed.

5.3.5 From the initial RF overdrive and dc breakdown measurements a number of important points were highlighted:

- During transmit operation it is desirable to bias the “off-state” LNA well into pinch-off such that RF induced voltage swings on the gate do not begin to turn the device “on” and degrade isolation (or in the extreme, destroy the device)
- Unfortunately the soft breakdown behaviour observed with the GaN samples, where the device degrades for reverse voltage swings  $>25V$ , is detrimental to the operation of an LNA required to withstand high levels of overdrive power.
- **This is a problem that has to be resolved if the full potential of GaN for high voltage withstand applications is to be realised.**

#### 5.4 Continuation of RF overdrive measurements

5.4.1 The dc breakdown measurements indicated that for reliable operation the critical reverse bias threshold voltage should not exceed 30V. Therefore, on this basis it was decided to repeat the RF overdrive tests with  $V_{ds}=0V$  and with the gate bias set at  $V_{gs}=-15V$  (i.e. halfway between its maximum voltage excursion for reliable operation).

5.4.2 With the GaN LNA in its “off state” it was found that an input power level of  $\approx 0.25W$  (5% duty cycle) could easily be achieved with no change in performance and that an input power level of  $\approx 0.5W$  (5% duty cycle) could be obtained, but with 1dB degradation in transmission isolation. Device destruction was found to occur for RF overdrive levels of  $\approx 4W$  (20% duty cycle), often due to catastrophic failure of a gate finger(s) as illustrated in figure 13-12.

5.4.3 From examining GaAs pHEMT LNA data sheets (for a similar size input device ( $2 \times 50 \mu m$ )), it appears that the maximum quoted input power level for reliable operation is in the region of 20 to 23dBm. Immature GaN technology appears to have the capability of exceeding the input power levels that are commonly accepted for GaAs device operation.

#### 5.5 Summary of key results from overdrive testing

5.5.1 In summary we have found that the GaN devices examined during the course of this project are not yet sufficiently electrically stable to be used as a replacement for the traditional PIN limiter/GaAs LNA combination in the receive path. The devices have displayed gradual RF gain degradation with increasing stress level, possibly associated with trapping in the device active region.

5.5.2 It is worth reiterating that the limits described above have been derived from measurements obtained on devices that were available at the start of this programme (2002). These are known to be from a less mature process than current GaN state-of-art, which has progressed since the available devices were fabricated. The operational limits given above are expected to improve significantly for stable GaN devices (i.e. stability on a par with present commercial GaAs devices). With such improvements it is felt that GaN technology offers considerable promise for realising robust receiver front-ends.

## **6 Transmit receive module system simulation (WP 2300 – Part 2)**

### **6.1 TRM modelling**

6.1.1 To reinforce the ideas presented in section 5, a system simulation study has also been undertaken to benchmark the potential benefits in using a GaN based LNA in an L-band radar Tx/Rx front end module (TRM). Both linear and non-linear CAD models, plus measured S-parameter data were used in conjunction with the Agilent ADS system simulation suite to undertake the evaluation.

### **6.2 Amplifier model**

6.2.1 Initially device S-parameter and noise parameter data was examined to determine the suitability of GaN devices for use in the L-band (1.2 to 1.3GHz) radar system scenario. From the device model for a 2x50µm gate width GaN transistor, various stabilisation and matching schemes were examined to implement a single stage LNA. Using either, (i) transformer – series inductor or (ii) lumped element C-L-C matching network topologies, similar amplifier results could be obtained. For operation at 1.25GHz ( $V_{ds}=20V$ ,  $V_{gs}=-5V$ ) the amplifier simulations have shown that a gain of 15.7dB and a noise figure of 1.38dB should be achievable. This is illustrated in figure 13-13.

### **6.3 TRM description**

6.3.1 The TRM front-end, shown schematically in figure 13-14, provides localized amplification of transmit and receive radar signals. In addition control of signal phase and amplitude is provided to allow beam shaping. The TRM will form part of an L-Band antenna assembly, which is required for a space borne SAR active phased array (L-SAR).

6.3.2 Functionally the module contains a >40W transmit chain and a pair of low noise receive chains (vertical and horizontal polarisation). The receive chains operate simultaneously to provide a fully polarimetric mode of operation. Phase and amplitude for the receive and transmit chains is adjustable to allow beam steering. The transmit path includes some gain adjustment for temperature effects and to compensate for amplitude variations with varying phase state.

6.3.3 Each module has a dedicated command and control ASIC. The L-SAR TRM also contains a calibration network, which can be commanded via the normal module command structure for use in the calibration of the whole radar system. The calibration routes power through the TX, RX or return path allowing each path to be measured in flight and compensation to be applied.

### **6.4 TRM ADS model**

6.4.1 The TRM modelling has made use of Agilent ADS CAD system models where they gave acceptable representation of a particular component function. However, a number of data files or custom components were also used to replace the ADS models where there were inaccurate or suffered convergence problems. Eight top level control schematics, varying

only in the sub-level items they reference and the receive (RX), transmit (TX), and calibration (CAL) state data used, were produced to simulate the following designs and functions:

- a. TRM with GaAs LNAs for RX (Receive) and operation with circulators.
- b. TRM with GaAs LNAs for RX (Receive) and operation with no circulators.
- c. TRM with GaN LNAs for RX (Receive) and operation with circulators.
- d. TRM with GaN LNAs for RX (Receive) and operation with no circulators.
- e. TRM with GaAs LNAs for TX (Transmit) and operation with circulators.
- f. TRM with GaAs LNAs for TX (Transmit) and operation with no circulators.
- g. TRM with GaN LNAs for TX (Transmit) and operation with circulators.
- h. TRM with GaN LNAs for TX (Transmit) and operation with no circulators.

6.4.2 The TX chain used was common to all the TRM schematic variants. It comprised of phase and gain control blocks, an S-band image rejection filter data file, a single GaAs LNA model and a driver amplifier followed by a p2d data file used to model the final power amplifier stage. This simulation chain produces the power to achieve >40W at the TRM output.

6.4.3 The models for the two RX chains in each TRM were specific to the technology of the LNA being investigated, GaN or GaAs. In the GaN case the difference between on and off states was implemented at the FET level with a switch routing power to the FET model or to a set of measured off-state S-parameters. This switching enables the off state  $S_{21}$  isolation and  $S_{11}$  signal return to be simulated in the TRM to ensure correct TX output power and CAL path simulation. A two stage GaN LNA was simulated by cascading two of the amplifier stages designed previously. This receiver chain configuration was compared with a GaAs MMIC LNA variant (designed by TNO FEL) incorporating an on-chip protection switch.

#### 6.4.4 Summary of ADS system simulation results

6.4.4.1 **Limiter removed:** Both GaN and GaAs LNA models have been fully evaluated in the ADS TRM model to describe transmit, receive and calibration modes of operation. The GaN LNA has proved as capable as the GaAs LNA in terms of gain and off state isolation, but with improved gain compression, power handling and hence noise figure due to the lack of requirement of a limiter.

6.4.4.2 **Limiter and circulator removed:** This simulation has shown that operation of a TRM without circulators offers major advantages in terms of improved system noise figure (0.75dB). However, the approach does increase the sensitivity of TX output power to the phase of the antenna signal return during beam-steering. The extent to which the phase change during beam-steering effects the TRM performance was not assessed due to lack of available antenna data.

**7 Low frequency noise (WP 3100 and WP 3200)**

**7.1 Rationale**

7.1.1 Results on the high frequency noise performance of GaN devices were presented in section 4. Work was also been undertaken to characterise GaN transistors in terms of their low frequency noise spectral density and to develop physical explanations for the measured results.

7.1.2 Low frequency (LF) noise measurements are important and are often made in order to help characterise integrated circuit (IC) fabrication processes. The LF noise reflects the transport properties of carriers and is also very sensitive to the presence of crystal defects in active layers and semiconductor interfaces. Therefore LF noise measurements can be used as a quality indicator of process technology.

**7.2 Measurement of low frequency drain and gate current noise**

7.2.1 Low frequency drain current noise measurements have been conducted on four GaN device variants to analyse excess noise contributions from the channel and access regions. The low frequency noise measurements have been performed over the 1Hz to 100kHz frequency range. An example of the experimental set-up used for the LF drain noise measurements is shown in figure 13-15 and comprises of a bias system, a very low noise amplifier, a spectrum analyser and a computer for data acquisition and processing.

**7.2.2 Typical measurements results**

7.2.2.1 Figure 13-16 shows a typical variation of the drain current noise spectral density measured at  $V_{gs}=0V$  with increasing drain current (i.e.  $V_{ds}$  is increased) for an MOVPE grown device on sapphire. A typical spectrum is composed of a  $1/f$  noise contribution for frequencies lower than 200Hz and a generation-recombination (G-R) noise component with a cut-off frequency around 10kHz. The G-R noise contribution reflects the activation of traps at room temperature. This type of measurement was undertaken for all device samples and a comparison of the normalised drain current noise at  $V_{gs}=0V$  in the ohmic region made.

7.2.2.2 The noise level in different materials and devices is usually characterised by the Hooge parameter. During the course of this work it has been verified that the  $1/f$  drain current noise increases with the square of the drain current in the ohmic region, thus verifying the Hooge relation given in equation 1.

$$S_{Id} = \alpha_H / N \cdot I_d^2 \cdot 1/f \quad \text{equation (1)}$$

7.2.2.3 Here,  $S_{Id}$  is the drain current noise spectral density,  $f$  is the frequency,  $N$  is the total number of electrons in the channel and  $\alpha_H$  is the Hooge parameter. From Ohms Law and for homogenous samples the number of carriers can be calculated from equation 2.

$$N=L_{DS}^2/q\mu R_{DS} \quad \text{equation (2)}$$

- 7.2.2.4 Here,  $\mu$  is the mobility of electrons in the conducting channel,  $R_{DS}$  is the total drain-source resistance and  $L_{DS}$  is the source-drain gap. For these devices, it was found that the ungated access regions between source and drain often dominated the noise, so we have considered  $N$  as the total number of electrons in the channel extending between source and drain and not only beneath the gate. On this basis the Hooge parameter was extracted for each technology and is compared in figure 13-17. This figure confirms the better quality, in terms of LF noise, of devices grown by MOVPE and MBE on sapphire substrates. It is also worth pointing out that the more recent MOVPE grown devices on SiC (variant 2) show a lower  $\alpha_H$  value in the same range as the devices on sapphire, possibly associated with the AlN exclusion layer used in this device.
- 7.2.2.5 In addition low frequency gate current noise measurements were also made. The accuracy of such measurements was restricted to a reduced frequency range dependent upon the level of noise current being measured, in some instances the data is only valid in the 1Hz to 500Hz range due to the test equipment noise floor. A typical gate noise spectral density measurement is shown in figure 13-18 for an MOVPE grown device on sapphire. Again, all devices exhibited  $1/f$  excess noise behaviour, with the white noise plateau commencing for frequencies  $>100\text{kHz}$ . The gate current noise was also found to include G-R noise contributions with a varying cut-off frequency dependent upon gate source voltage.
- 7.2.2.6 In general it was found that the  $1/f$  gate current noise spectral density ( $S_{ig}$ ) increased with decreasing  $V_{gs}$  (i.e. more negative  $V_{gs}$ ) and hence with increasing reverse bias gate leakage current. Moreover, devices with high levels of gate leakage were found to have a higher level of  $1/f$  noise.
- 7.2.2.7 Unfortunately it was found that the variations in the  $I_g$ - $V_{gs}$  characteristics between different technologies, and between devices of the same technology, prevented identification of a clear mechanism responsible for the LF gate noise.

### 7.3 Low frequency noise modelling

- 7.3.1 The dependence of current noise sources on transistor bias has been analysed and physical modelling proposed. The main contributions to the drain noise were analysed in the ohmic and saturated regions of the IV characteristic with varying  $V_{gs}$ . The contributions coming from the ungated and gated regions of the device were separated and the regimes where each were dominant identified. Then the possible correlation between the gate and drain noise and the contribution of gate current fluctuation to output noise was investigated. It was found that at high gate leakage ( $>\mu\text{A}$ ), there was full correlation between gate and drain current noise, with no correlation at low gate current. The details of this modelling exercise are described further in reference [8].

## 8 Oscillator phase noise comparison (WP 3300)

### 8.1 Rationale

8.1.1 Oscillator phase noise occurs due to the upconversion of low frequency noise around the microwave carrier signal. To achieve low levels of phase noise it is important to minimise low frequency noise in the intrinsic semiconductor material/device structure.

8.1.2 From a system perspective, achieving low levels of oscillator phase noise is essential for low bit error rate (BER) in modern communication systems and for realising high sensitivity doppler radars. In order to gain a qualitative understanding of how GaN technology could potentially offer improvements in phase noise it is useful to consider the expression for oscillator single sideband phase noise, equation 3, developed by Robins [10].

$$L(f_m) = 10 \log \left( \frac{FkT}{C} \cdot \frac{1}{8Q^2} \cdot \left( \frac{f_o}{f_m} \right)^2 \right) \quad \text{equation (3)}$$

8.1.3 Here, C refers to the output power, Q is the loaded quality factor of the resonator feedback circuit, F is the noise figure of the forward gain loop amplifier,  $f_o$  is the carrier frequency and  $f_m$  is the offset frequency relative to the carrier frequency. It can be seen that phase noise is inversely proportional to output power and the loaded quality factor of the resonator. Maximising these parameters will automatically minimise phase noise [11]. Hence if the 1/f baseband noise and upconversion mechanisms for GaN are comparable with GaAs, there is **also** the potential for reduced oscillator phase noise due to the five fold increase in output power offered by GaN active device technology. Therefore the main aim of this work package was to investigate the phase noise performance of oscillators realised using GaN HFET devices.

### 8.2 Choice of active device

8.2.1 It was decided early on in the project that the chosen oscillator test vehicle would be designed in a modular format such that different active devices could be used in the oscillator breadboard. For this work it was decided to compare the performance of a 10GHz DRO oscillator realised using GaN HFET, GaAs FET and SiGe bipolar technology.

8.2.2 Four device types were chosen for evaluation. These consisted of two GaN device variants (GaN on SiC variant 1 and variant 2), a SiGe HBT (Infineon BFP 620) and a GaAs pHEMT (Transcom TC1401). The latter devices were chosen to allow a comparison of relatively mature technology to be made with GaN.

### 8.3 Oscillator topology

- 8.3.1 The basic oscillator topology adopted was a parallel feedback design consisting of an amplifier stage and a high Q filter feedback network, realised using a dielectric resonator (DR). This topology, as opposed to a series feedback reflection oscillator, was chosen since it was felt to be a more repeatable and robust oscillator design approach that can be (i) easily adjusted to satisfy the Barkhausen Criterion and (ii) allow ease of comparison of different device technologies. A 10dB coupler was included on the output to buffer the oscillator from non-ideal 50ohm loads in order to minimise frequency pulling effects.
- 8.3.2 Particular care was taken in the design of the oscillator breadboard to ease performance comparison across different device technologies. To allow a direct comparison of performance it is important to use the same resonator, the same circuit housing and to equalise loop gain for the different active devices. This was achieved by designing the oscillator motherboard to accept drop-in carrier substrates containing different active device types.
- 8.3.3 Each active device was mounted on a 250µm thick aluminium nitride (AlN) carrier tile containing 50Ω input and output microstrip lines and source/emitter ground via holes. AlN was chosen since it has a much higher thermal conductivity (170W/m.K) than alumina, aiding heat dissipation for the GaN devices. A photograph of one of the active device carriers, containing a 2x50µm, gate width GaN HFET, is shown in 13-19. Upon completion of die attach and the addition of source bonds, S-parameter measurements were made using an RFOW probe station to give accurate model data for the assembly.
- 8.3.4 A photograph of the complete oscillator is given in figure 13-20. The resonator cavity can be clearly seen at the top of the photograph, while the bottom half of the breadboard contains the forward gain loop amplifier section and the replaceable carrier used for examining each active device type.
- 8.3.5 The oscillator motherboard was constructed using brass backed duroid (Rogers RT 5880, 127µm thick) since its low dielectric constant ( $\epsilon_r=2.2$ ) made placement and replacement of the DR puck less critical on the phase change around the loop. The gate and drain of the active device were biased separately allowing an independent analysis of frequency, power and phase noise in terms of bias variation.

### 8.4 Measured results

- 8.4.1 Output power and phase noise measurements were undertaken to evaluate oscillator performance for each device type using a spectrum analyser and Agilent's E5500 Phase Noise Measurement System.
- 8.4.2 An overlay of measured phase noise performance for each active device variant is given in figure 13-21. As expected the SiGe HBT has the lowest phase noise performance out of all the device types examined with a value of  $-135\text{dBc/Hz}$  at a 100KHz offset. The next best phase noise performance was obtained from the GaAs pHEMT device ( $-123\text{dBc/Hz}$ ) followed by GaN variant 2 ( $-118\text{dBc/Hz}$ ) and GaN variant 1 ( $-110\text{dBc}$ ). To

the best of our knowledge the phase noise result for the GaN variant 2 oscillator is the lowest yet reported for this technology.

8.4.3 Both GaN technology variants exhibit a constant 30dB/decade reduction in phase noise with increasing offset frequency (until the equipment measurement noise floor is reached). This rate of phase noise variation is due to the up conversion of low frequency (LF) noise sources in the semiconductor material onto the carrier frequency. 20dB/decade in variation comes from equation 3 and 10dB/decade from the 1/f noise dependence of the LF noise. An improvement of 5-8 dB in phase noise was measured between the different GaN device variants, and is entirely consistent with the baseband 1/f noise measurements. The difference in noise is believed to be the result of a developing technology with improvements in material growth and device structure. The AlN barrier layer present in variant 2 will reduce tunnelling into the AlGaIn layer, reducing the 1/f noise by limiting the number of traps which are accessible to channel electrons.

8.4.4 A summary of measurement results is shown in table 12-8. It can be seen that a higher level of output power was achieved with GaN variant 2 (17.3dBm) compared with GaN variant 1 (11.7dBm). Oscillator output power levels of 16.6dBm and 4.8dBm were obtained from the GaAs pHEMT and SiGe HBT device configurations respectively. It is interesting to point out that similar oscillator output power levels were obtained for the Transcom GaAs pHEMT and the GaN variant 2 device. However, the GaN device used has a gate width that is a factor of 12 smaller than the GaAs device, corresponding to a 14 fold improvement in output power density.

- With improvements in material quality the low frequency noise performance of GaN based oscillators is likely to improve further allowing high power, low phase noise oscillators to be realised.

## 9 Conclusions

- 9.1 This report summarises the key results from the ESA project “Noise Assessment of Gallium Nitride Structures” (reference A0/1-3916/01/NL/CK) covering the period from May 2002 to January 2004. The objective of this work programme was to perform a study of GaN field effect transistors in order to gain an improved understanding of the intrinsic noise sources.
- 9.2 Three different material growth systems have been characterised during the course of this work to determine their RF and low frequency noise properties. These were MOVPE growth on SiC, including two layer variants (variant 1 (GaN/AlGa<sub>N</sub>) and variant 2 (GaN/AlN/AlGa<sub>N</sub>)), MOVPE growth on sapphire and MBE growth on sapphire. Additional work items have included a system study to evaluate the benefits of using GaN for realising an L-band Tx/Rx module and evaluation of the phase noise performance of a 10GHz oscillator.
- 9.3 **High frequency measurements :** RF characterisation of a range of device samples has shown that the gain and noise figure performance of GaN devices is comparable to what is achievable from GaAs device technology. For a 2x50 $\mu$ m, 0.25 $\mu$ m gate length, MOVPE grown device on SiC, a minimum noise figure of  $\approx$ 1dB was achieved at 10GHz with >12dB associated gain. For a 2x75 $\mu$ m, 0.6 $\mu$ m gate length MBE grown device on sapphire a value of 3.8dB and 8dB was achieved respectively. With device optimisation it is likely that the noise figure of these GaN devices could be reduced further. In addition it has been shown that for high V<sub>ds</sub> operation, GaN devices grown on silicon carbide (SiC) are preferable to sapphire due to the higher thermal conductivity offered by this material.
- 9.4 **High frequency noise modelling:** Noise models (using a small signal FET equivalent circuit and additional gate and drain current noise sources) have been developed which accurately describe measured RF noise behaviour as a function of frequency and bias. It was found that the drain current noise source is independent of frequency and of drain-source voltage (V<sub>ds</sub>) in the range 10-20V, and increases approximately linearly with drain current, but less rapidly than in a GaAs device of similar gate length. The magnitude of the drain current noise for samples on SiC and for the best samples on sapphire was approximately 10% of that expected for ideal shot noise. The magnitudes of the gate current noise sources were found to be smaller than the drain noise sources. They corresponded to shot noise produced by gate leakage currents of a few  $\mu$ A. For the MBE devices, the magnitude of the gate current noise source was found to be much higher than used to model the MOCVD grown devices. This was not surprising since gate current leakage was found to be relatively high for the MBE samples examined.
- 9.4.1 Unfortunately it was not possible to obtain a meaningful interpretation of the origin of the physical RF noise sources. Further measurements on devices with longer gate lengths and with different concentrations of aluminium in the Schottky layer are required.

- 9.5 **Evaluation of the use of GaN in a TR module :** A CAD based system simulation study has been completed to benchmark the potential benefits in using a GaN based LNA in an L-band transmit/receive (Tx/Rx) front-end. In particular these simulations have considered the feasibility of removing the limiter and circulator functions in terms of voltage breakdown and in terms of noise figure improvement. For both scenarios the system simulations have shown that there is the potential to achieve a 1 to 1.5dB improvement in system noise figure due to a reduction in ohmic insertion loss. However, with the limiter and circulator removed the effect of varying phase angle, during beam steering, on TR module performance still needs to be addressed.
- 9.5.1 To experimentally validate the feasibility of removal of the limiter function in a GaN receiver chain, RF overdrive measurements were also performed. These measurements were made on a GaN LNA in order to emulate what might happen during the transmit cycle of a radar system. This was achieved by subjecting the LNA, biased in its “off-state”, to increasing levels of RF input power. With the gate heavily reverse biased it was found that the devices exhibited gain degradation as RF input power was increased. DC reverse bias breakdown measurements were then made to examine in more detail the effect of increasing reverse bias voltage on device behaviour. For reverse voltage swings >25V it was found that the GaN device samples showed an irreversible soft breakdown behaviour, preventing the devices from withstanding high levels of output power.
- **Gate soft-breakdown is a problem that has to be resolved if the full potential of GaN for high voltage withstand applications is to be realised.**
- 9.5.2 Even so, it was possible to demonstrate reliable operation with input power levels of 23dBm without any performance change and up to 27dBm with 1dB degradation in the off-state isolation of the device. These values are felt to be higher than can be achieved using GaAs technology.
- 9.5.3 It is worth emphasising that the limits described above have been derived from measurements obtained on devices that were available at the start of this programme (2002). These are known to be from a less mature process than current GaN state-of-art, which has progressed since the available devices were fabricated. The operational limits given above are expected to improve significantly for stable GaN devices (i.e. stability on a par with present commercial GaAs devices).
- **With such improvements it is felt that GaN technology offers considerable promise for realising robust receiver front-ends.**
- 9.6 **Low frequency noise :** Low frequency noise (1Hz to 100KHz) measurements were made to give an indication of the “quality” of the GaN processing technology. Low frequency drain and gate current noise measurements were completed on four device variants. It was found that the drain and gate noise spectrums typically consisted of a 1/f noise contribution and a generation-recombination noise component (probably associated with the activation of traps at room temperature). The Hooge parameter ( $\alpha_H$ ) was

extracted for each technology and indicated the better quality, in terms of LF noise, of devices grown by MOVPE and MBE on sapphire substrates. It was also found that the more recent MOVPE grown devices on SiC (variant 2) showed an  $\alpha_H$  value in the same range, possibly associated with the AlN exclusion layer used in this device.

**9.7 X-band oscillator demonstration :** Achieving low levels of oscillator phase noise is important in high performance communication links and in doppler radar systems. It occurs as a result of low frequency baseband noise being upconverted in the active device. If the  $1/f$  baseband noise and upconversion mechanisms for GaN are comparable to GaAs then there is the potential for reduced oscillator phase noise as a result of the increased available output power. Hence, the aim of this work was to construct a GaN based oscillator and evaluate its phase noise performance.

9.7.1 A 10GHz dielectric resonator oscillator test vehicle, with removable transistor carriers, was designed to allow the phase noise performance of GaN device samples to be compared with GaAs FET and SiGe bipolar technology. Four device types were chosen for evaluation in the oscillator breadboard. These consisted of two GaN device variants (variant 1 and variant 2), a SiGe HBT (Infineon BFP 620) and a GaAs pHEMT (Transcom TC1401). The latter devices were chosen to allow a comparison of relatively mature technology to be made with GaN.

9.7.2 Output power and phase noise measurements were undertaken using a spectrum analyser and Agilent's E5500 Phase Noise Measurement System. As expected the SiGe HBT had the lowest phase noise performance out of all the device types examined with a value of  $-135\text{dBc/Hz}$  at a 100KHz offset. The next best phase noise performance was obtained from the GaAs pHEMT device ( $-123\text{dBc/Hz}$ ) followed by GaN variant 2 ( $-118\text{dBc/Hz}$ ) and GaN variant 1 ( $-110\text{dBc}$ ). Both the GaN oscillator variants were found to have a constant 30dB/decade reduction in phase noise with increasing offset frequency and suggests that the oscillator phase noise is dominated by the upconversion of low frequency noise sources. For the GaN device samples it is worth pointing out that an improvement in phase noise of 5-8dB was obtained from device variant 2 which was consistent with the baseband  $1/f$  noise measurements. The difference in noise is believed to be due to the result of a developing technology with improvements in material growth and device structure occurring over time.

- **With improvements in material quality the low frequency noise performance of GaN based oscillators is likely to improve further allowing high power, low phase noise oscillators to be realised.**

## 9.8 Summary

9.9 Wide bandgap semiconductors have many properties that are near ideal for electronic and optical applications requiring high temperature, high frequency, high power and radiation hardness. To-date most researchers have concentrated their efforts on examining the high frequency output power capability of transistors manufactured using the gallium nitride (GaN) material base. This work has shown that GaN device technology offers gain and noise performance comparable to that achievable with GaAs, but with breakdown voltages exceeding 60V. These results suggest an important new application area for

GaN as robust low-noise amplifiers, where the high breakdown voltage offers the potential for removal of front-end protection devices.

- 9.10 System simulation has shown that it could be feasible to remove the limiter and possibly the circulator functions for an L-band phased array radar system with advantages in terms of system noise figure, component cost and mass. However, experimental overdrive measurements have shown that there may be a soft breakdown effect that needs to be resolved before the full potential of GaN based receivers can be realised. Low frequency noise and oscillator phase noise measurements have given an indication of the status of processing/material quality compared with mature device technologies such as GaAs and SiGe. It is clear that improvements in material growth and device process technology are still required.
- 9.11 Over time these material improvements are likely to occur and it is therefore concluded that GaN offers exciting possibilities for realising high power amplifiers and highly robust receiver front-ends.

**10 Acknowledgements**

10.1.1 The author wishes to thank Paul Rice for oscillator design and characterisation, Mark Black for assistance with module build and Francois Garat (ESA) for his enthusiasm throughout the project. We would like to thank Ana Jimenez and Elias Munoz of UPM, Madrid for the devices on MBE GaN material used in this project.

## 11 References

1. ESA ITT reference AO/1-3916/01/NL/CK, August 2001
2. QinetiQ bid proposal, "Noise assessment of gallium nitride structures", QinetiQ/MMS/MS/BID/22/002, October 2001.
3. A Barnes, D Hayes, "Technical Note 1 : RF Characterisation Results", QinetiQ/S&E/OPC/CR02021416/2.0, July 2003.
4. W A Phillips, "ESA GaN Noise Assessment – Technical Note 2", QinetiQ/S&E/OPC/CR030375/1.0, September 2003.
5. D Hayes, "Technical Note 3 – Overdrive test results", QinetiQ/S&E/OPC/TN030714/1.0, April 2003.
6. A Knight, G Cobb, "Technical Note 4 – TRM RF low noise front-end feasibility and perspective", ENG-TCN-EU-03-0122, January 2004.
7. N Malbert, A Curutchet and N Labat, "Technical Note 5 – Electrical characterisation of low frequency noise", 04011/GaN/NM/NL, January 2004.
8. N Malbert, A Curutchet and N Labat, "Technical Note 6 – Study of low frequency noise sources", 04012/GaN/NM/NL, January 2004.
9. A Barnes, "Technical Note 7 – Oscillator phase noise comparison", QinetiQ/S&E/OPC/CR040296/1.0, January 2004.
10. W.P. Robins, Phase noise in signal sources, London: Peter Peregrinus Ltd, 1982
11. M J Underhill, "Reduction of phase noise in single transistor oscillators," IEE European Frequency Time Forum, March 1996.

12 Tables

System	Substrate	
	Sapphire	SiC
MOVPE grown AlGa <sub>N</sub> (variant 1)	Bookham 2x50μm device, QinetiQ material	Bookham 2x50μm device, QinetiQ material
MOVPE grown AlGa <sub>N</sub> with AlN exclusion layer (variant 2)		QinetiQ 2x50μm device, QinetiQ material
MBE grown AlGa <sub>N</sub> /Ga <sub>N</sub>	Madrid University 2x75μm device, Madrid University material	

Table 12-1; Device structures examined

Device	Temp.	F <sub>t</sub> (GHz)	F <sub>tmax</sub> (GHz)	MAG/MSG (dB) @ 10GHz	NF (50ohm) (dB) @10GHz	NF <sub>min</sub> (dB) @ 10GHz	Associated Gain (dB) @ 10GHz	Breakdown voltage (V)
MOVPE on SiC W <sub>g</sub> =2x50μmL g=0.25μm V <sub>ds</sub> =20V, V <sub>gs</sub> =-5V	25°C	33.5	83.5	12.9	7.4	1.15	12.1	>60V
	150°C	30.4	75.6	12.5	6.2			
MOVPE on sapphire W <sub>g</sub> =2x50μmL g=0.25μm V <sub>ds</sub> =10V, V <sub>gs</sub> =-4V	25°C	31	86.6	12.1		2.5	12.2	>60V
	150°C	13	37.7	8.5	Device failure			

Table 12-2; Summary of MOVPE device performance (Variant 1)

Device type	T (°C)	I <sub>g</sub> (mA)	I <sub>d</sub> (mA)	F <sub>t</sub> (GHz)	F <sub>tmax</sub> (GHz)	MAG/MSG (dB) @ 10GHz	NF (50ohm) (dB) @10GHz	NF <sub>min</sub> (dB) @ 10GHz	Associated Gain (dB) @ 10GHz	Breakdown voltage (V)
MBE on sapphire W <sub>g</sub> =2x75μmL g=0.6μm V <sub>ds</sub> =15V, V <sub>gs</sub> =-7V	25	-0.06	13.2	17.9	45.5	10.5	8.75	3.82	9	>25V
	150	-0.24	6.67	12.9	34.5	7.53	9.86	5.71	7.1	>25V

Table 12-3; Summary of MBE device performance

**Caswell HFET Vds=20V (variant 1)**

V <sub>GS</sub> (V)	I <sub>DS</sub> (mA)	I <sub>DS</sub> /I <sub>DSS</sub>	$\langle i_d^2 \rangle$ (pA <sup>2</sup> )/Hz	$\langle i_g^2 \rangle$ (pA <sup>2</sup> )/Hz
0	88	1.0	1300	1.4
-1	82	0.93	1050	1.8
-2	74	0.84	1000	1.3
-3	65	0.74	730	2.0
-4	53	0.60	620	1.7
-5	38	0.44	380	1.3
-6	22	0.25	220	0.3

Table 12-4; Gate and drain noise current source strength versus I<sub>ds</sub> (MOVPE on SiC variant 1)

**Device Yankee 11-05, Vds=10V (variant 2)**

V <sub>gs</sub> (V)	I <sub>ds</sub> (mA)	I <sub>ds</sub> /I <sub>dss</sub>	$\langle i_d^2 \rangle$ (pA <sup>2</sup> )/Hz	$\langle i_g^2 \rangle$ (pA <sup>2</sup> )/Hz	I <sub>g</sub> (μA)
0	113	1.0	250	0	+4
-1	103.6	0.92	200	0	0
-2	90.0	0.80	250	0	7
-3	75.2	0.67	380	0.2	13
-4	59.9	0.53	350	3	18
-5	43.8	0.39	270	3	22
-6	23.8	0.21	180	2	26

**Device Yankee 10-07, Vds=10V (variant 2)**

V <sub>gs</sub> (V)	I <sub>ds</sub> (mA)	I <sub>ds</sub> /I <sub>dss</sub>	$\langle i_d^2 \rangle$ (pA <sup>2</sup> )/Hz	$\langle i_g^2 \rangle$ (pA <sup>2</sup> )/Hz	I <sub>g</sub> (μA)	$\langle v^2 \rangle$ (nV <sup>2</sup> )/Hz
-2	110.8		470	0	-8	0.5
-3	95.5		440	0	-12	0.3
-4	79.1		440	0	-17	0.1
-5	60		500	0	-24	0
-6	39		390	0	-29	0
-7	16.9		280	0	-44	0

**Device: Yankee 10-07, Vds=15V (variant 2)**

V <sub>gs</sub> (V)	I <sub>ds</sub> (mA)	I <sub>ds</sub> /I <sub>dss</sub>	$\langle i_d^2 \rangle$ (pA <sup>2</sup> )/Hz	$\langle i_g^2 \rangle$ (pA <sup>2</sup> )/Hz	I <sub>g</sub> (μA)
-2	109.6		1100	0	-8
-3	96.5		1000	0	-12
-4	80.0		900	0	-21

Table 12-5; Gate and drain noise current source strength versus I<sub>ds</sub> (MOVPE on SiC variant 2)

**Unlimited**

$V_{gs}$ (V)	$I_{ds}$ (mA)	$I_{ds}/I_{dss}$	$I_g$ ( $\mu$ A)	$\langle i_d^2 \rangle$ ( $pA^2$ )/Hz	$\langle i_g^2 \rangle$ ( $pA^2$ )/Hz
-3	47.3		102	650	25
-4	39.7		71	400	30
-5	31.8		68	400	20
-6	23.0		62	400	15
-7	13.2		56	200	15

*Table12-6; Gate and drain noise current source strength versus  $I_{ds}$  (MBE on sapphire)*

Parameter	Ref 1	Ref 2	Ref 3	Ref 4	Ref 5	Ref 6a	Ref 6b
$NF_{min}$ at 12GHz (dB)	1.1	0.9	0.75	0.8	1.2	0.8	1.2
$G_{ass}$ at 12 GHz (dB)	10	11	10	11	12	11	8
$f_T$ (GHz)				38	42	58	35
Drain bias voltage (V)	10	6	10	15	20	1	1
Drain current (mA)	11	40	15	12	22	10	10
Device width ( $\mu$ m)	100	200	100	100	100	150	150
Source-drain gap ( $\mu$ m)	2	2	2	3	3	2	2
Gate length (nm)	250	150	120	200	200	150	150
Al conc (%)	30		20	25	25		
Transconductance (mS)	22	60	18	17	17	34*	20*
Substrate	SiC	SiC	SiC	sapp	SiC	SiC	SiC
$\langle i_d^2 \rangle$ ( $pA^2$ /Hz)				200	220	250	250

*Table 12-7; Publication analysis for low noise GaN devices (for sub-references see [4])*

Parameter	GaN HFET on SiC Variant 1	GaN HFET on SiC Variant 2	GaAs pHEMT	SiGe HBT
Pout (dBm)	11.7	17.3	16.6	4.8
Power density (mW/mm)	148	537	38	-
SSB Phase noise (dBc) @100kHz	-110	-118	-123	-135

*Table 12-8; Summary of oscillator measurement results*

13 Figures

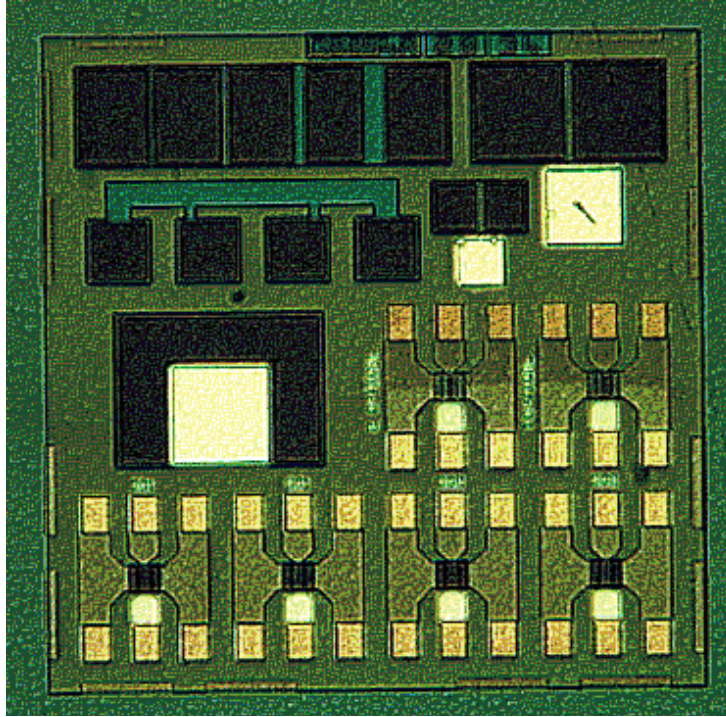


Figure 13-1; Photograph of Bookham device field (MOVPE on SiC)

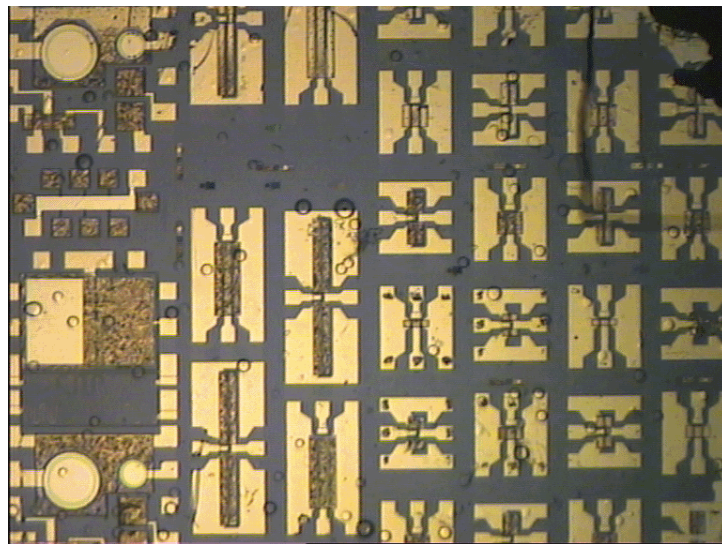


Figure 13-2; Photograph of Madrid University device field (MBE on sapphire)

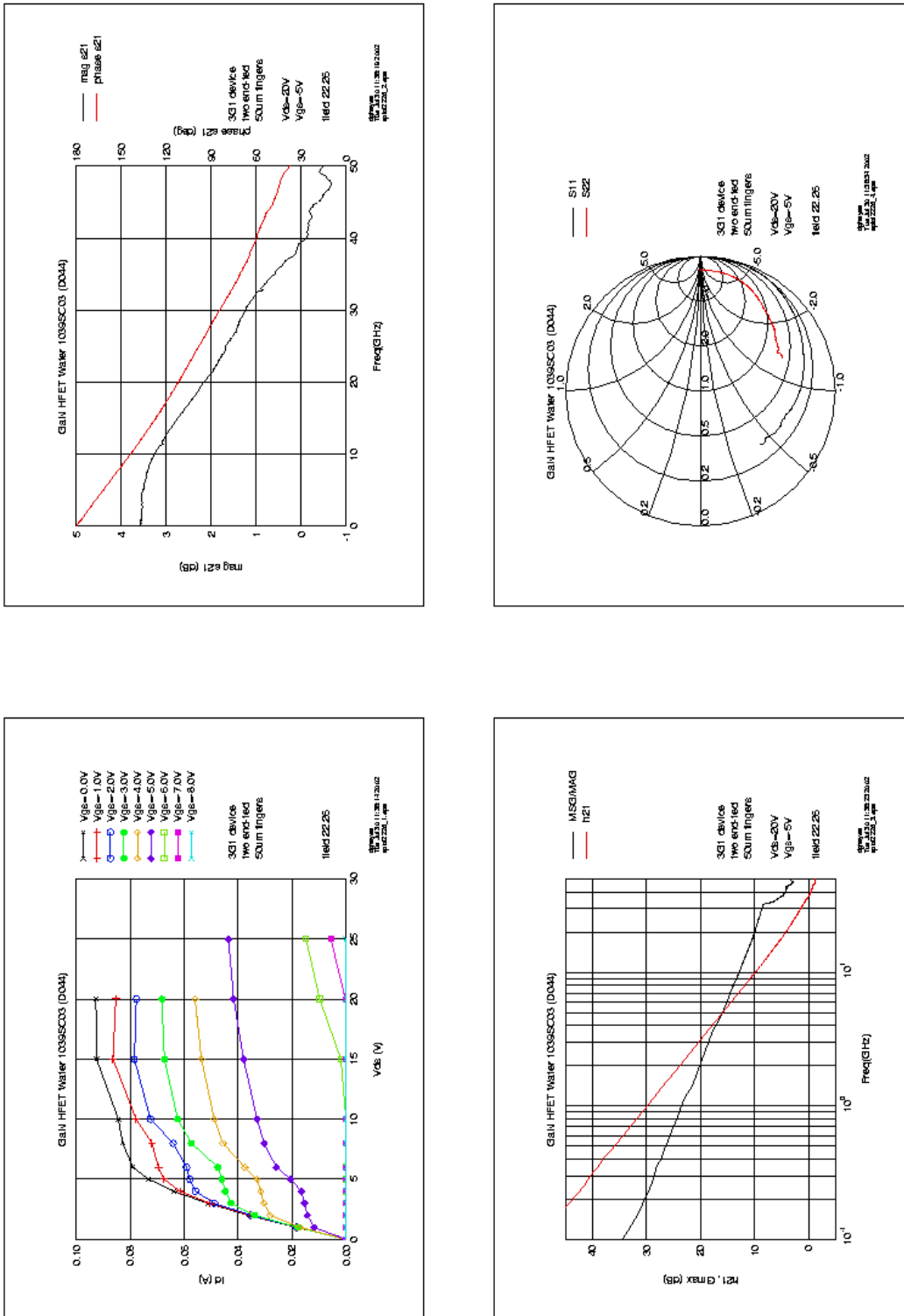


Figure 13-3; S-parameter data for MOVPE device on SiC (variant 1,  $V_{ds}=20V$ ,  $V_{gs}=-10V$ ,  $T=25^\circ C$ )

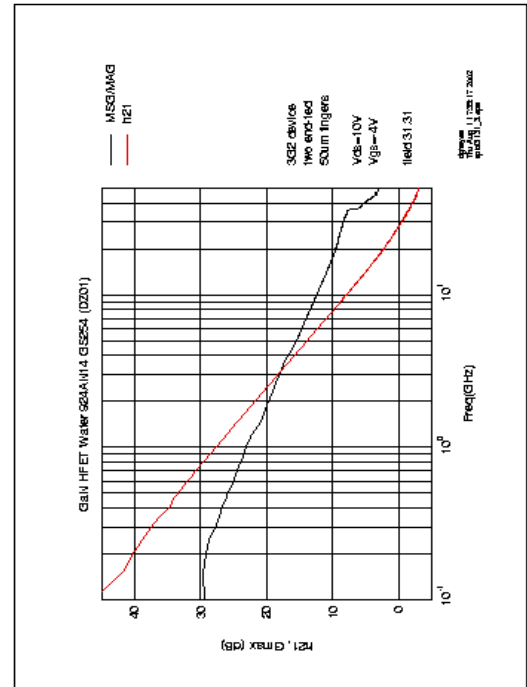
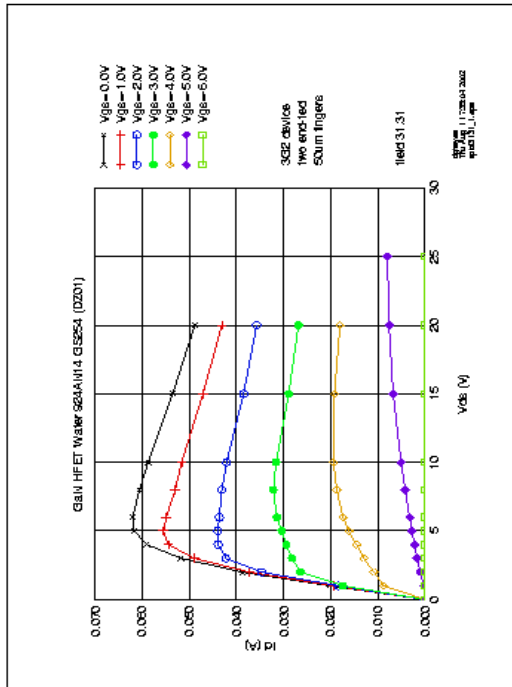
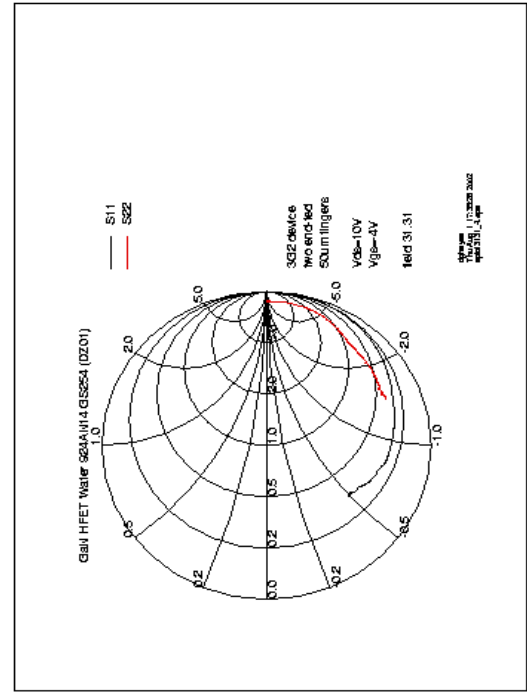
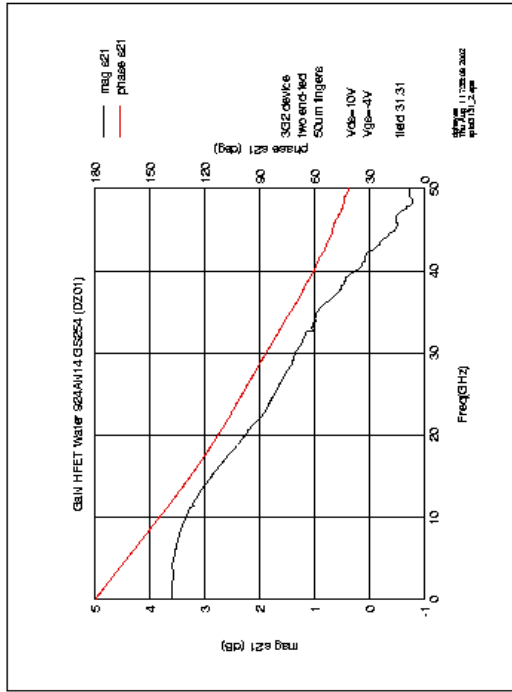


Figure 13-4; S-parameter data for MOVPE device on sapphire (variant 1,  $V_{ds}=10V$ ,  $V_{gs}=-4V$ ,  $T=25^{\circ}C$ )

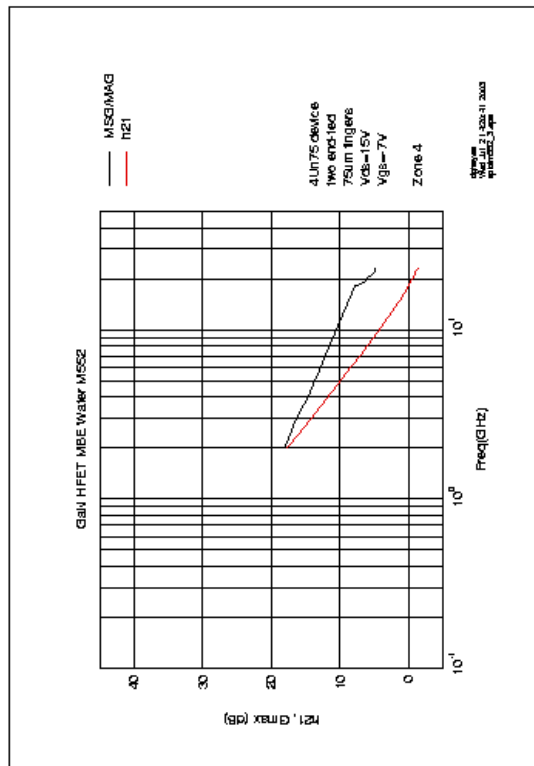
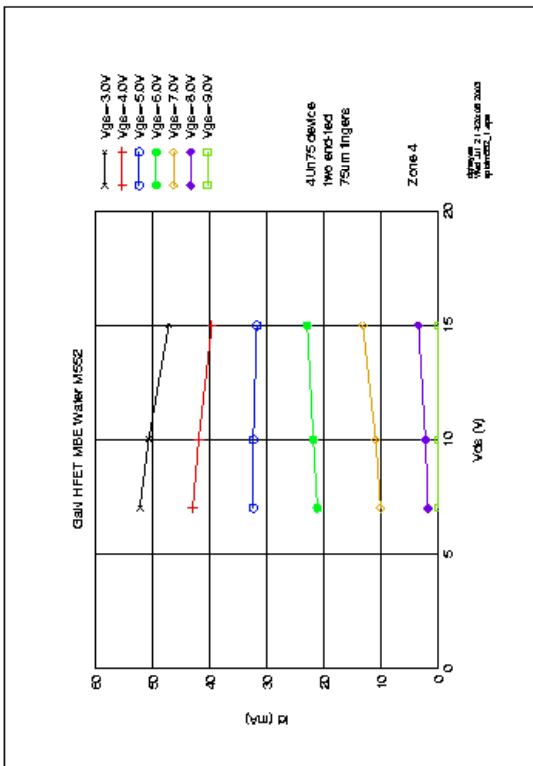
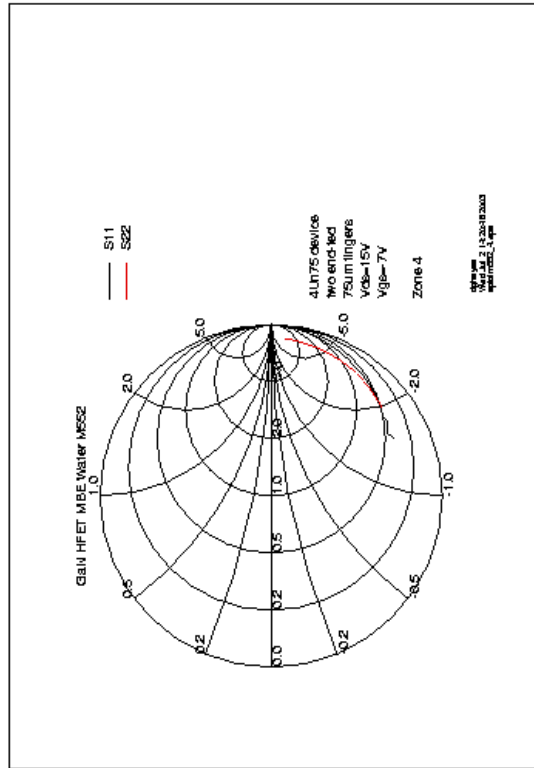
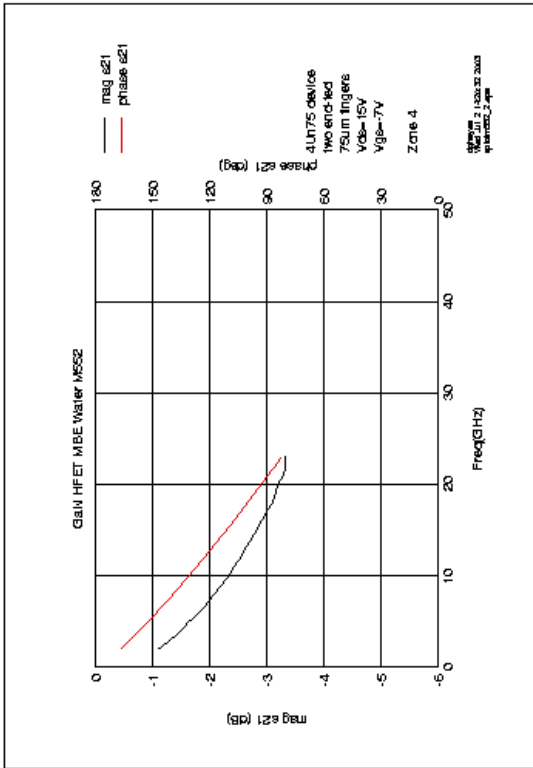
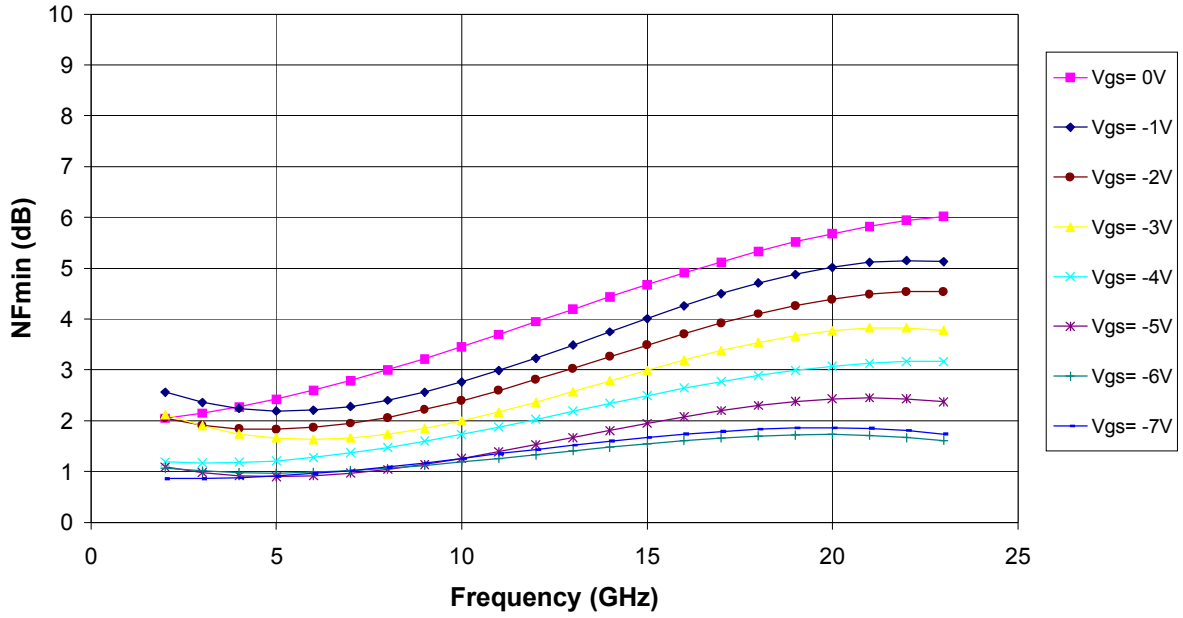


Figure 13-5; S-parameter data for MBE device on sapphire (4Un75, Vds=15V, Vgs=-7V, T=25°C)

SiC substrate 1039SC03 3G1 X26.Y21 Vds= 20V



SiC substrate 1039SC03 3G1 X26.Y21 Vds= 20V

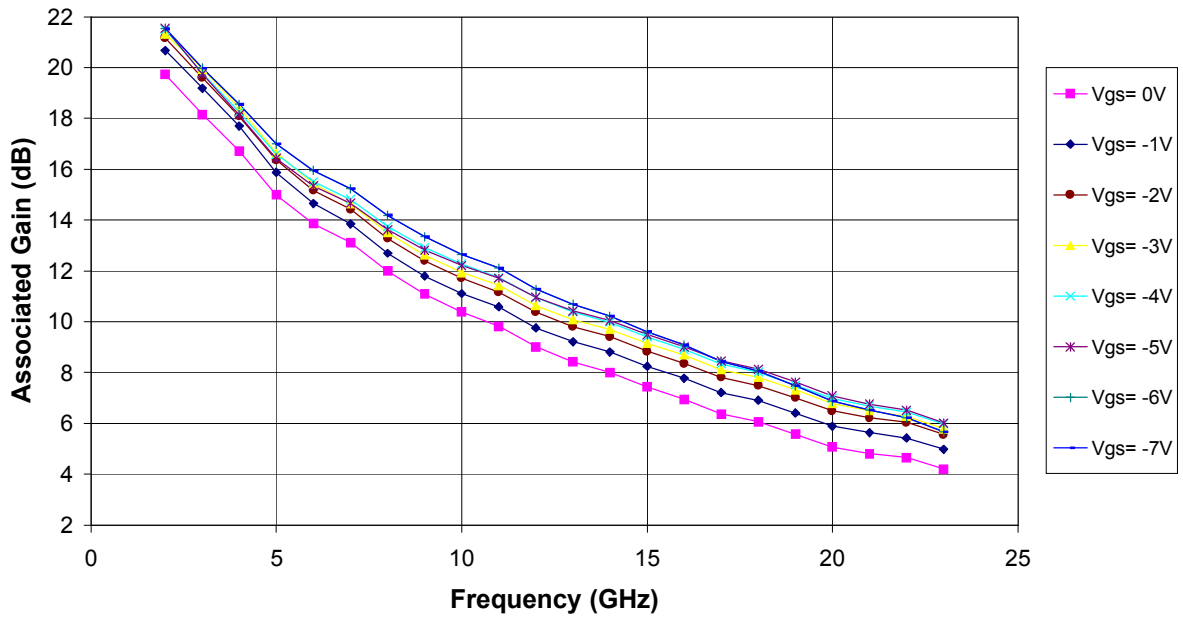


Figure 13-6; NFmin and associated gain for MOVPE device on SiC, Variant 1 (Vds=20V, T=25°C)

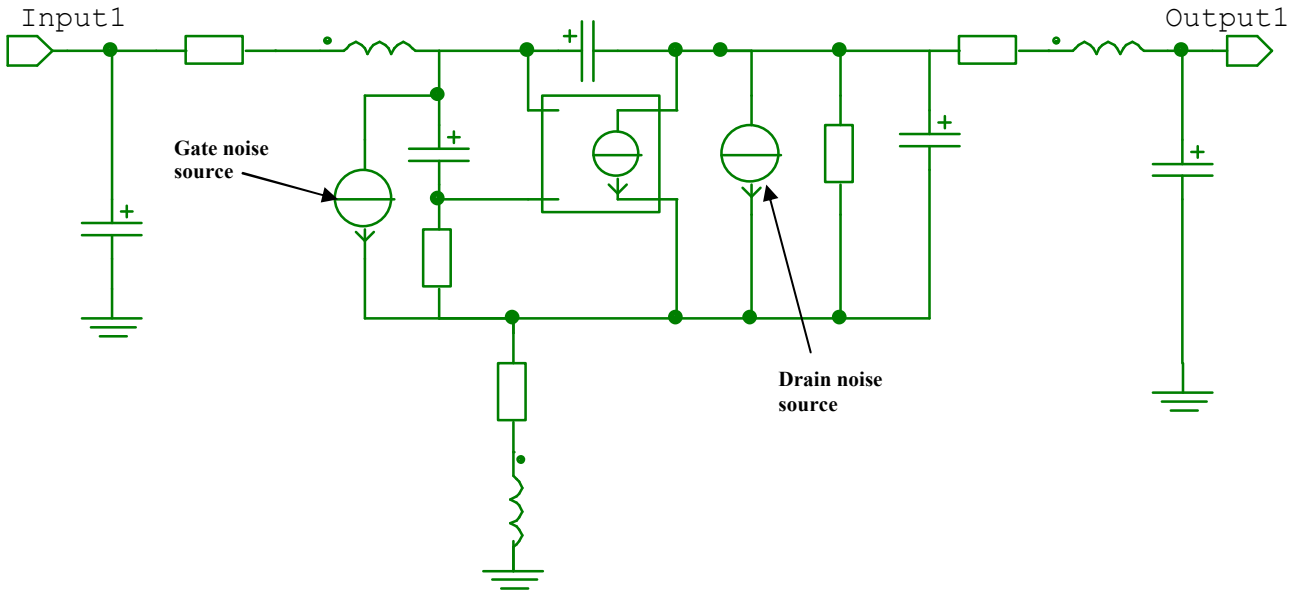


Figure 13-7; Schematic of HFET model used for noise and S-parameter analysis

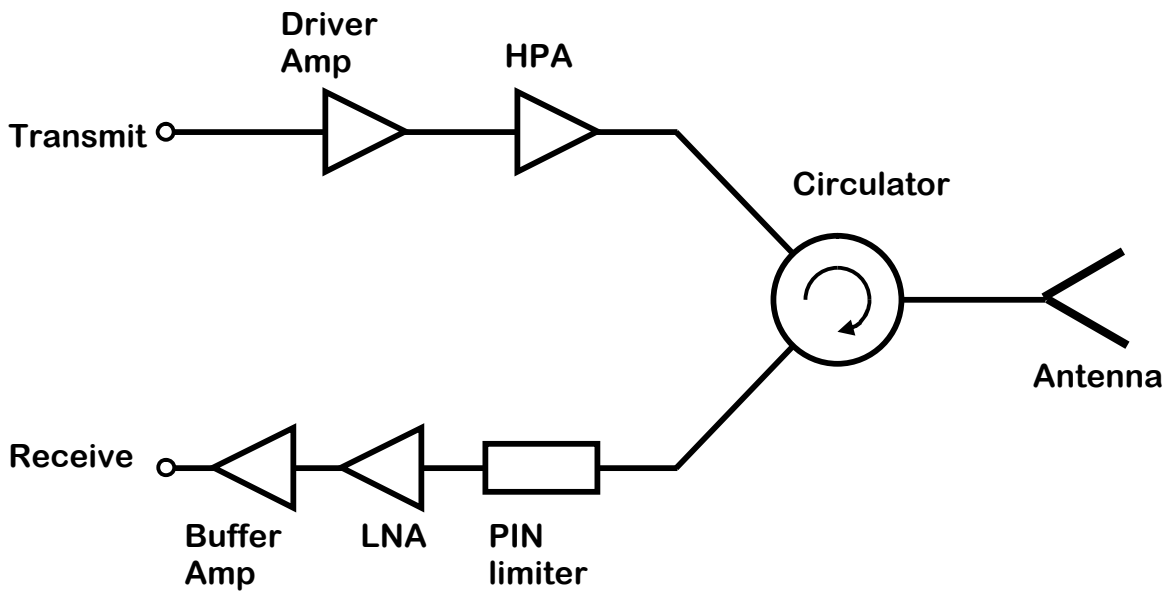


Figure 13-8; Typical transmit-receive architecture

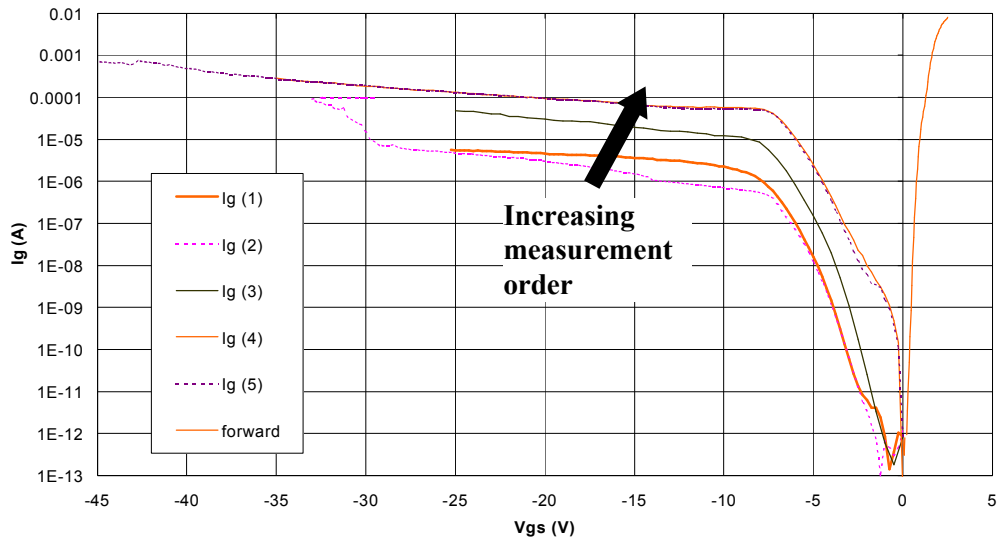


Figure 13-9; Gate-source breakdown behaviour for MOVPE device on SiC, Variant 1 (22.36 3G1)

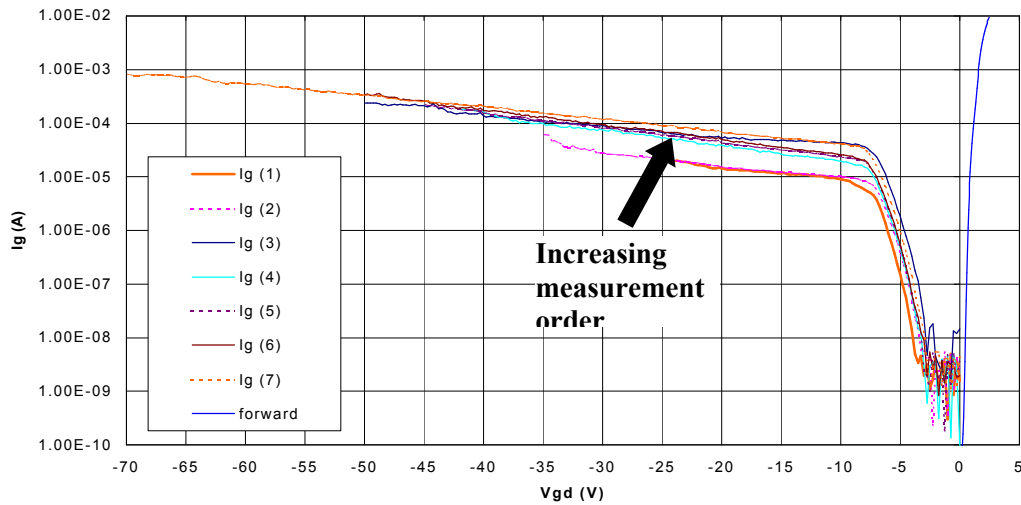


Figure 13-10; Gate-drain breakdown behaviour for MOVPE device on SiC, Variant 1 (22.36 3G1)

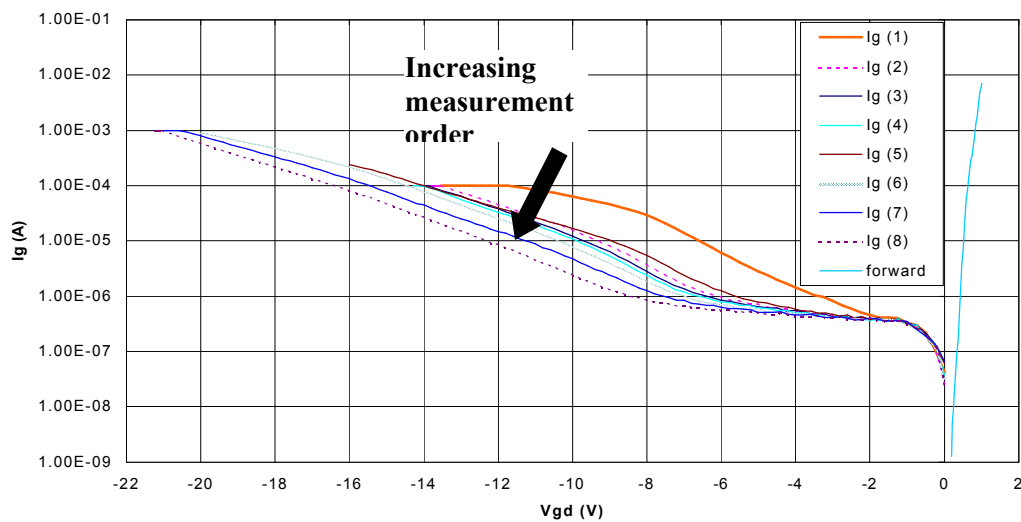


Figure 13-11; Gate-drain breakdown voltage behaviour for Bookham H40P GaAs pHEMT

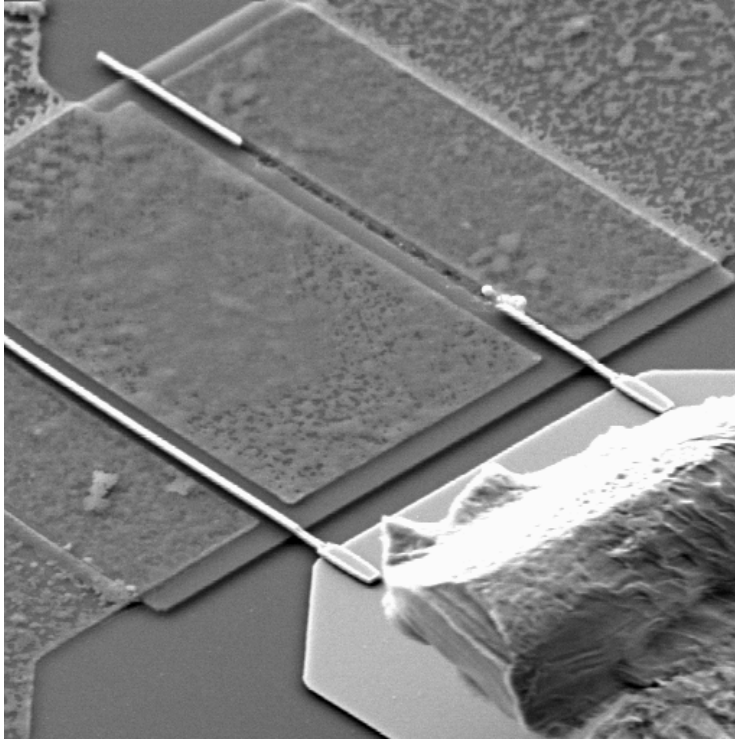


Figure 13-12; Example photograph showing typical gate finger failure during isolation testing

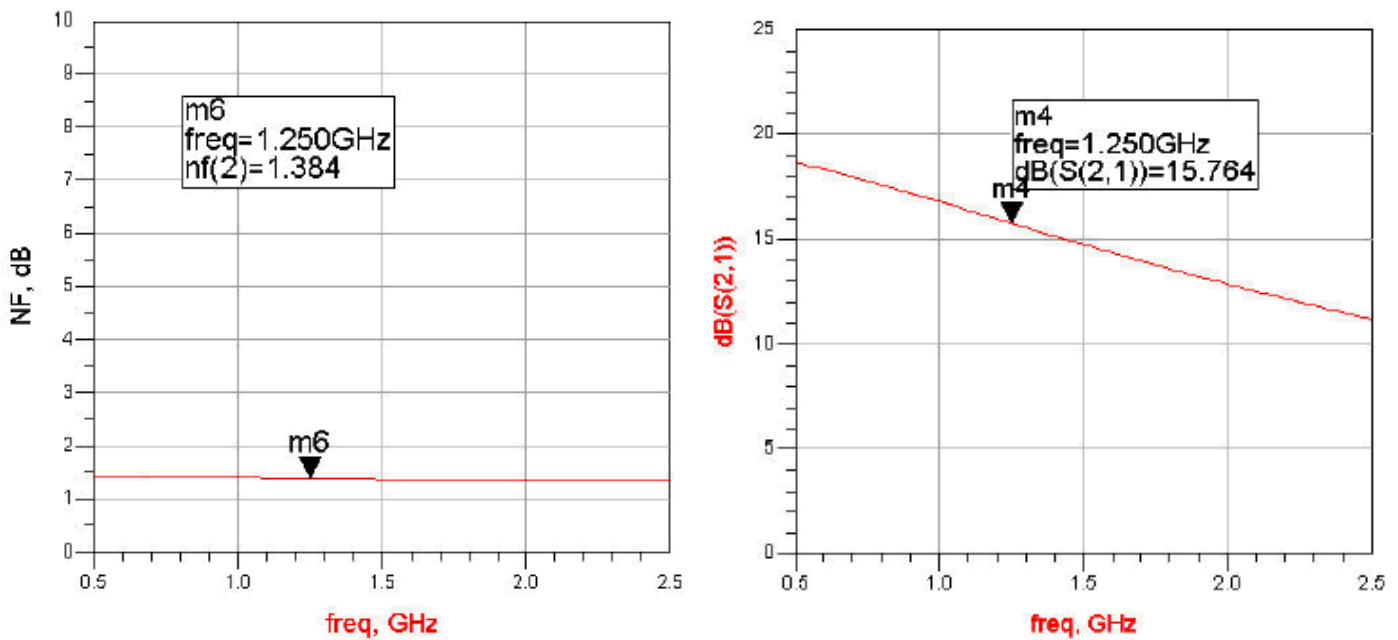


Figure 13-13; Simulated GaN LNA noise figure/gain (stabilised, transformer matching network)

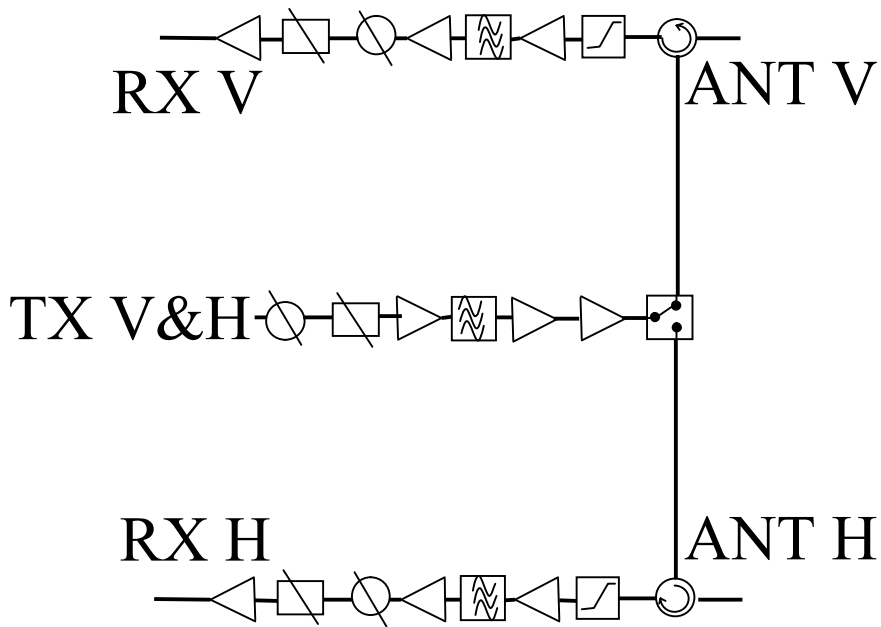


Figure 13-14; Astrium L-band SAR radar diagram (including circulator and limiter)

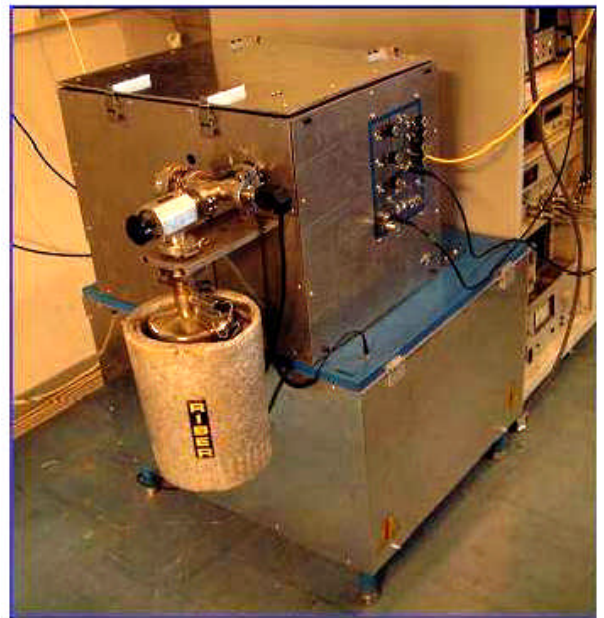
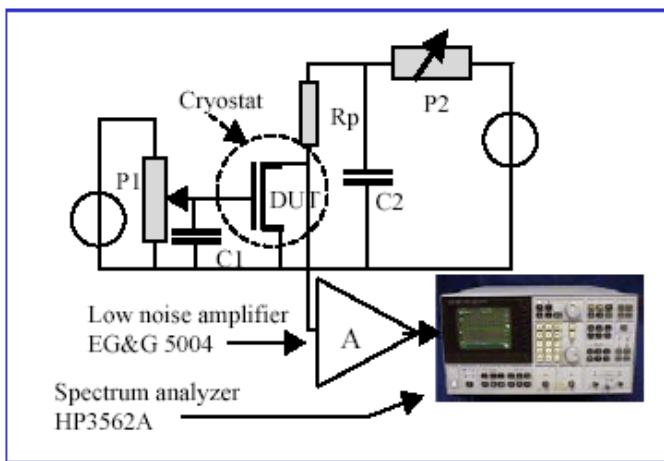


Figure 13-15; Experimental set-up for LF drain current noise measurements

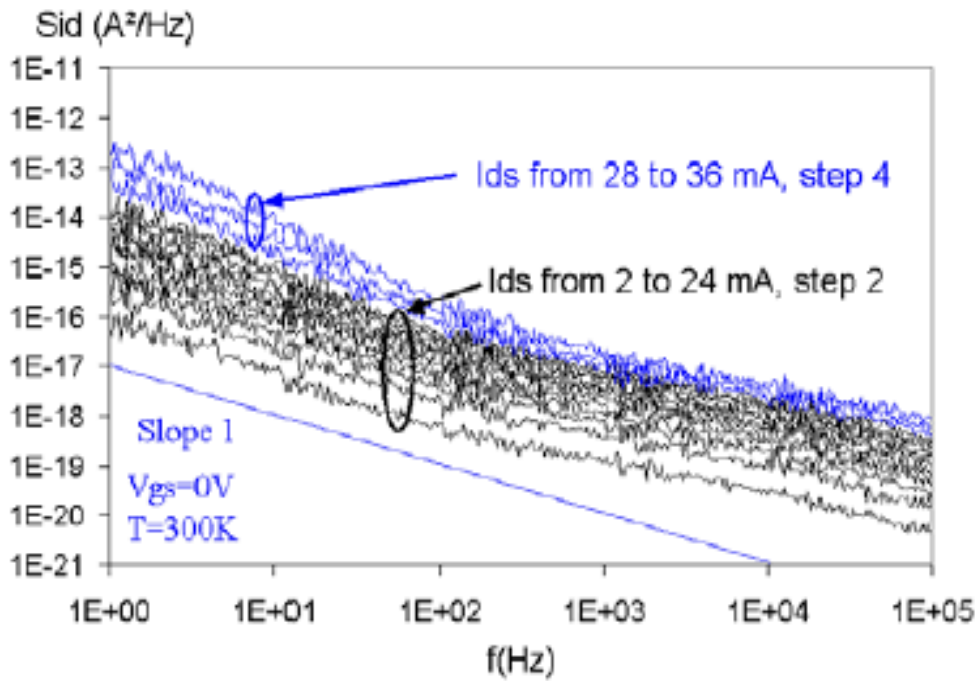
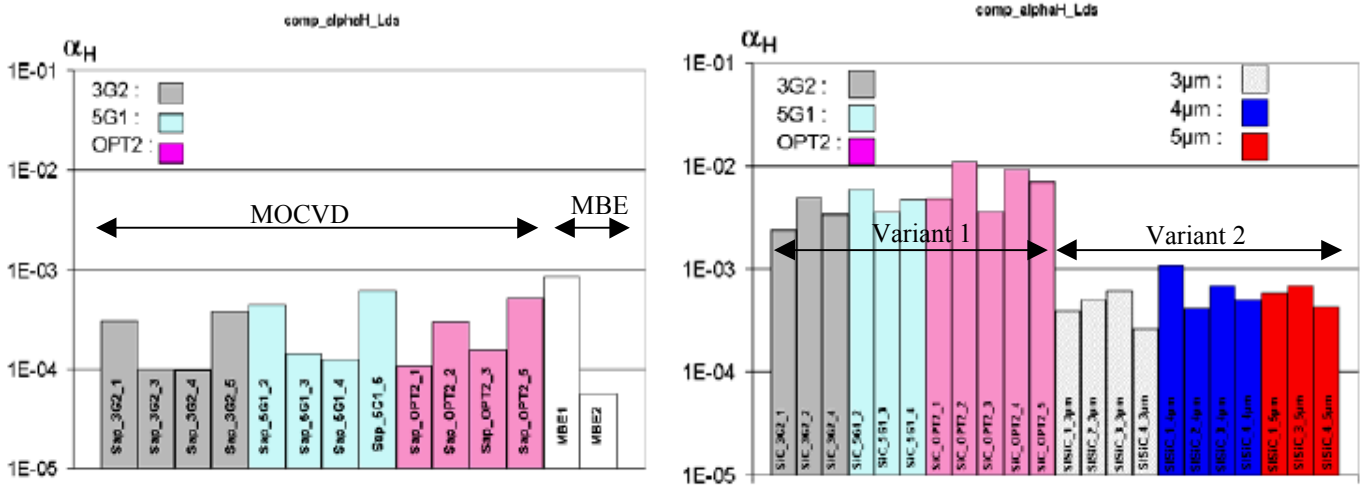


Figure 13-16; Typical drain current noise spectral density with  $I_{ds}$  at  $V_{gs}=0$  (MOVPE device on sapphire)



(a) MOCVD devices on Sapphire, and MBE devices on Sapphire

(b) MOCVD devices on SiC (1<sup>st</sup> and 2<sup>nd</sup> technologies)

Figure 13-17; Comparison of Hooge parameter ( $\alpha_H$ ) for each device technology

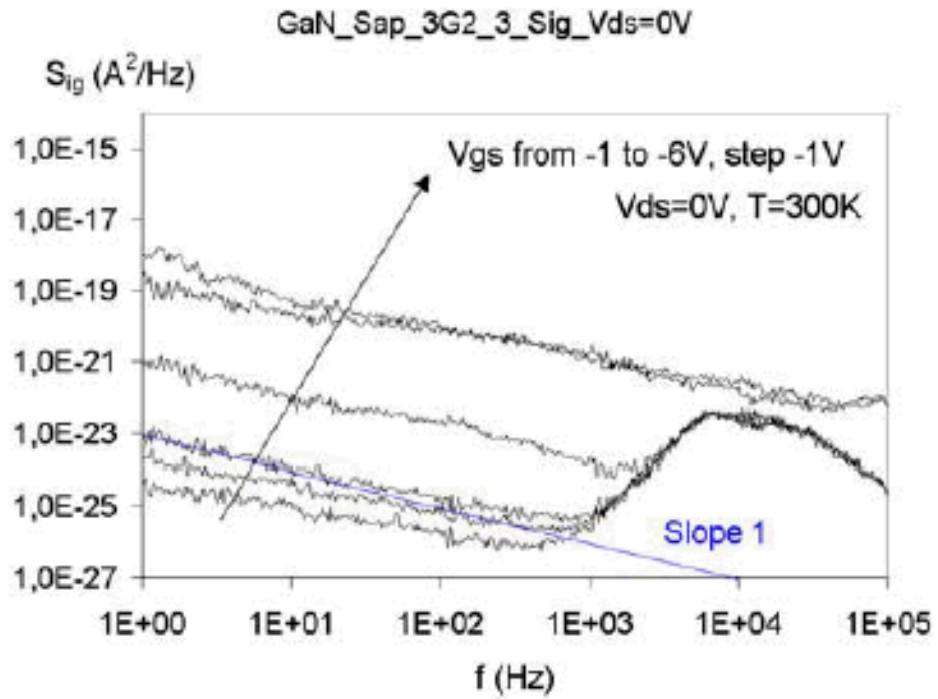


Figure 13-18; Typical variation in gate current noise spectral density with  $V_{gs}$ ,  $V_{ds}=0V$  (MOVPE device on sapphire,  $I_g$  varying from  $-1.2nA$  to  $-0.24\mu A$ )

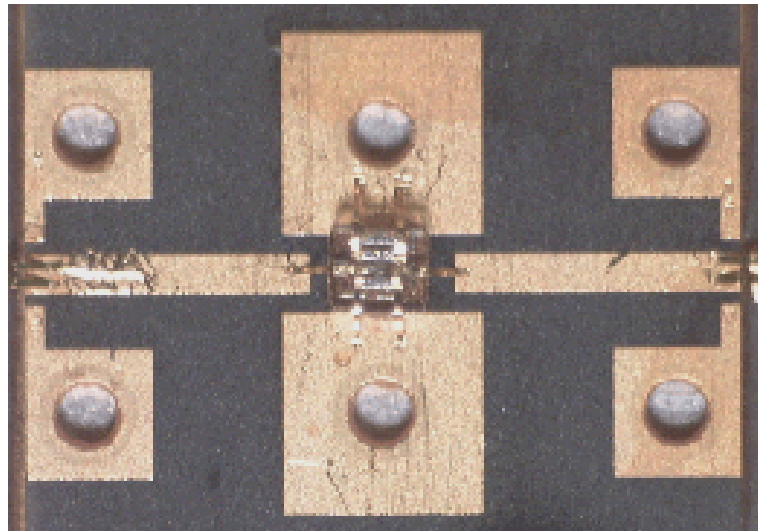


Figure 13-19; Aluminium nitride drop-in carrier containing GaN device

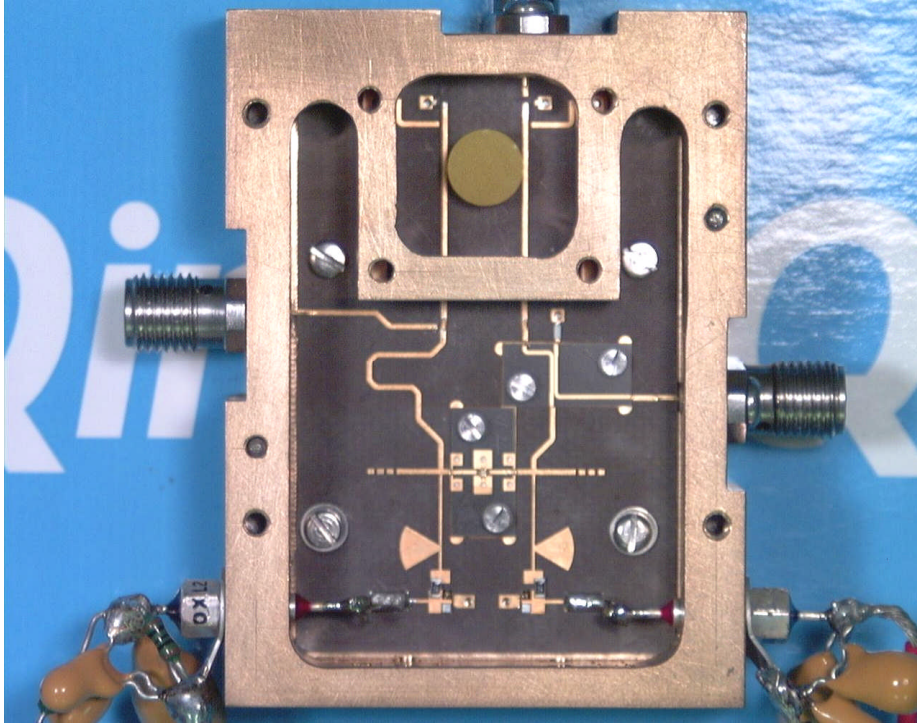


Figure 13-20; Photograph of 10GHz oscillator breadboard

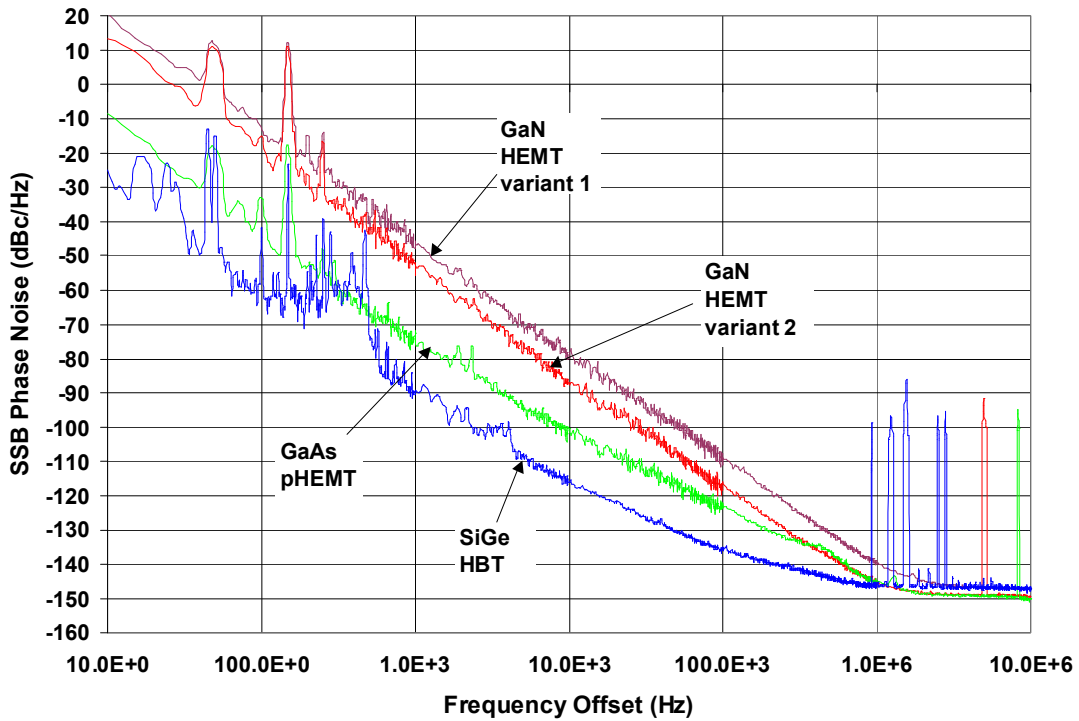


Figure 13-21; Oscillator phase noise using SiGe bipolar, GaAs pHEMT and 2 GaN HFET on SiC variants

**Report documentation page**

1. Originator's report number:		QINETIQ/S&E/OPC/CR041056/1.0	
2. Originator's Name and Location:		A R Barnes PA113, QinetiQ, Malvern, England	
3. Contract number and period covered:		ESTEC Contract No. 15908/01/NL/CK	
4. Sponsor's Name and Location:			
5. Report Classification and Caveats in use:		6. Date written:	Pagination:      References:
QinetiQ Proprietary - Authorised Distribution Only		April 2004	x + 42      11
7a. Report Title:		ESA GaN Noise Assessment - Summary Report	
7b. Translation / Conference details (if translation give foreign title / if part of conference then give conference particulars):			
7c. Title classification:		UC	
8. Authors:		A R Barnes	
9. Descriptors / Key words:		<b>GALLIUM NITRIDE, LOW NOISE, RF OVERDRIVE, OSCILLATOR, PHASE NOISE, 1/F NOISE</b>	
10a. Abstract. (An abstract should aim to give an informative and concise summary of the report in up to 300 words).			
<p>This report summarises the key results from the ESA project “Noise Assessment of Gallium Nitride Structures” (reference A0/1-3916/01/NL/CK) covering the period from May 2002 to January 2004. The objective of this work programme was to perform a study of GaN field effect transistors in order to gain an improved understanding of the intrinsic noise sources. Three different material growth variants have been characterised during the course of this work to determine their RF and low frequency noise properties. Additional work items have included a system study to evaluate the benefits of using GaN for realising an L-band Tx/Rx module and evaluation of the phase noise performance of a 10GHz oscillator.</p>			
10b. Abstract classification:		FORM MEETS DRIC 1000 ISSUE 5	

**Unlimited**

**This page is intentionally blank**

**Unlimited**